FUEL CYCLE OPTIMIZATION OF A HELIUM-COOLED, SUB-CRITICAL, FAST
TRANSMUTATION OF WASTE REACTOR WITH A FUSION NEUTRON SOURCE

A Thesis Presented to
The Academic Faculty

By

James Warren Maddox

In Partial Fulfillment
Of the Requirements for the Degree
Master of Science in Nuclear Engineering

Georgia Institute of Technology

May, 2006

FUEL CYCLE OPTIMIZATION OF A HELIUM-COOLED, SUB-CRITICAL, FAST
TRANSMUTATION OF WASTE REACTOR WITH A FUSION NEUTRON SOURCE

Approved by:

Dr. Weston Stacey, Advisor
School of Mechanical Engineering
Georgia Institute of Technology

Dr. Nolan Hertel
School of Mechanical Engineering
Georgia Institute of Technology

Dr. Edward Hoffman
Nuclear Engineer
Argonne National Laborotory

Date Approved: March 9, 2006

ACKNOWLEDEMENTS

TABLE OF CONTENTS

LIST OF TABLES

LIST OF FIGURES

SUMMARY

Possible fuel cycle scenarios for a helium-cooled, sub-critical, fast reactor with a fusion neutron source for the transmutation of spent nuclear fuel have been analyzed. The transmutation rate was set by the 3000MWth fission power output. The primary objective was to achieve >90% burn of the transuranic (TRU) fuel obtained from spent nuclear fuel. A secondary objective was to examine the possibility of achieving this "deep burn" without reprocessing after initial fabrication of the TRU into coated particle TRISO fuel.

Four sets of 5-batch fuel cycle scenarios, differing in the constraints imposed on the beginning of cycle (BOC) k-eff and the end of cycle (EOC) neutron source strength (characterized by the fusion neutron source power level), were evaluated. In scenario A, k_{eff}^{BOC} was required to be 0.95 and P_{fusion}^{EOC} < 200 MWth was required. In scenario B, the k_{eff}^{BOC} restriction was removed to allow less reactive BOC fuel loadings, while the 200 MW upper limit on P_{fus}^{EOC} was retained.

It was found that the primary objective of > 90% TRU burn-up could be achieved by repeatedly reprocessing the TRISO TRU fuel particles to remove fission products and add fresh TRU "makeup" at the end of each 5-batch burn cycle, without needing to increase the fusion neutron source power above 100 MWth when the k_{eff}^{BOC} is restricted to 0.95.

The secondary objective of obviating processing could only be accomplished when the k_{eff}^{BOC} restriction was removed and recycling was employed or when both k_{eff}^{BOC} and P_{fus}^{EOC} restrictions were removed in a single-pass "deep burn" fuel cycle. In scenario C, with both the k_{eff}^{BOC} limit and the fusion power limit unrestricted, >90% TRU burn-up was achieved

without reprocessing the TRISO TRU fuel particles, which could then be buried intact in a high-level waste repository, but a neutron source rate $P_{fus}^{EOC} \approx 3370$ MWth was required. In scenario D, with only the k_{eff}^{BOC} limit unrestricted, >90% TRU burn-up was achieved without reprocessing by the continuous recycle of TRISO particles through the reactor.

CHAPTER 1: INTRODUCTION

Five decades of commercial nuclear power production in the United States have created approximately 50,000 MT of spent nuclear fuel (SNF) distributed at numerous locations throughout the country, a number which will continue to increase by 2,000 MT/year at the present level of nuclear power production [1]. In order to provide a permanent repository for spent fuel from commercial nuclear reactors and government sources (defense and Department of Energy), the Yucca Mountain Project was undertaken to create a high-level waste repository with a capacity of 70,000 MT. At the current rate of SNF production, a new storage facility comparable to the Yucca Mountain facility would be required every 34 years [2].

Repository capacity is determined primarily by decay heating, which for SNF after several hundred years in which the short-lived fission product radioactivity decays substantially is primarily due to the remaining long-lived TRU. If the TRU content of SNF could be reduced, the long term decay heat would be reduced, the repository capacity would be increased, and the time until a new repository following Yucca Mountain is needed would be lengthened. Since the most abundant SNF TRU, plutonium, may also be used in nuclear weapons, TRU reduction in SNF also constitutes an increase in proliferation resistance as it destroys any incentive for intrusion and diversion. The only known method of destruction of the TRU is via neutron fission, the energy release from which could be used to generate electricity.

There may be both "criticality" and safety advantages to sub-critical operation of transmutation reactors. Sub-critical operation with a neutron source rate that can be

1

increased to compensate for the negative reactivity caused by fissile depletion and fission product build-up should be advantageous in obtaining deep burn-up of the TRU. It will also entail infrequent or no reprocessing.

The dominance of plutonium in the TRU content of the SNF (see table 1) indicates that a TRU fuel extracted from SNF will have a smaller delayed neutron fraction ($\beta = 0.020$ for Pu239, $\beta = 0.064$ for U235 [3]) than equivalent U-235 fuel. In a critical reactor, the "margin of safety" for accidental reactivity insertions (i.e. the value of reactivity for which a prompt critical runaway excursion occurs) is β, but in a reactor operating sub-critical by $\Delta k = 1 - k_{eff}$ the margin of safety is the considerably larger value $\beta + \Delta k$.

Table 1. TRU portion of SNF – principal isotopes.

Isotope	Mass %
NP237	4.34%
PU238	1.25%
PU239	54.10%
PU240	21.34%
PU241	3.89%
PU242	4.69%
AM241	9.23%
AM243	1.03%
CM244	0.12%

Research interest in SNF transmutation has focused on both accelerator-driven systems [1, 4-8] and, to a much lesser extent, on fusion-driven systems [9-19]. The Accelerator Transmutation of Waste (ATW) Roadmap, as requested by the United States Congress in 1999, evaluated the status and potential of, and proposed a path of development for, accelerator-driven transmutation sub-critical systems. This study concluded that the use of an ATW system to transmute LWR SNF would destroy 99.9% of its TRU content and reduce the radiation dose of a repository such as the proposed facility at Yucca mountain by a factor of 10 [1].

Hoffman and Stacey [2] performed a comparative evaluation of the impact on repository performance of repeated recycling of TRUs in fast sub-critical transmutation reactors driven by both accelerator and fusion neutron sources and in critical fast transmutation reactors, relative to the once-through LWR fuel cycle and to a one-pass MOX (mixed oxide) recycle. They found: 1) that repeated recycle of TRUs through fast transmutation reactors would produce a waste stream with substantially reduced repository heat removal requirements and increased proliferation resistance, the toxicity of which would reduce to approximately that of uranium ore within about 500 years; 2) that the net transmutation rate of TRU-fueled sub-critical fast reactors driven by accelerator and fusion neutron sources were comparable, but that both were significantly greater than the net transmutation rate of comparable TRU-U fueled critical fast reactors.

There have been relatively few comparative studies of accelerator- and fusion-driven sub-critical transmutation reactors. Parish and Davidson [9], in a study that evaluated the feasibility of fission product transmutation using fusion reactors, noted that while both accelerator-driven systems and fusion-driven systems produce an abundant source of neutrons necessary for transmutation, accelerator-driven systems will likely consume a great deal of energy, while fusion-driven transmutation can potentially produce a great deal of energy. This same general conclusion was found in subsequent studies by Stacey [15] and Jassby and Schmidt [19].

The fusion neutron source has another advantage over the accelerator-spallation neutron source due to the distribution of the source over a large volume resulting in less demanding heat removal requirements and radiation damage limits [16, 17]. And although the primary objective is the destruction of TRUs, it is worth noting that for Q > 2, a fusion-

driven system has a larger heat production capacity relative to an accelerator-driven system and thus a larger net electricity production rate for a given TRU destruction rate [15]. And since such a tokamak need only drive a sub-critical system, the performance requirements are less demanding than for a fusion device intended for power production and are within the ken of the current tokamak operational database, indicating that such a tokamak is practicable subject to availability requirements of at least 50% [15, 17].

Several exploratory studies of transmutation of spent nuclear fuel with sub-critical reactors driven by fusion neutron sources have been performed. Peng and Cheng [11] investigate the electricity generating capacity of a fusion-driven transmutation system to determine the practicality of small fusion devices employed to transmute nuclear waste in high epi-thermal flux regions. Cheng and Cerbone [12] analyzed and compared two tokamak based transmutation reactors: (1) minor actinide (MA) fueled and (2) "Pu-assisted" (Pu+MA fuel) which they determined could operate at a Pfus=200 MW, k-eff ~0.8 and Pfus=75 MW, k-eff ~0.9, respectively. Stacey, et al. [19] developed a metal fuel, liquid metal cooled, sub-critical transmutation of waste reactor driven by a tokamak neutron source with a 4-batch fuel cycle that achieved a discharge burn-up of 25% per cycle with a cycle time of 623 days, P_{fusion}^{EOC} of 150 MW and k_{eff}^{BOC} of 0.95.

The use of the coated TRISO particle adds an additional level of containment that introduces the possibility of "deep burn" of TRU fuel without reprocessing. This is because the TRISO layers form a corrosion-resistant pressure vessel that serves to contain the fission products (FPs) released during irradiation and for millions of years afterwards in storage, in wet or dry conditions [21, 22], thus making the TRISO particle an attractive choice for deep burn transmutation and long-term storage provided the particles can withstand the high

irradiation levels concomitant to deep burn. Rodriguez, et al. [22] investigated a deep-burn, thermal spectrum, modular helium critical reactor (MHR) using for the TRU component of LWR SNF in TRISO particles. Very high burn-ups (>65% Pu, >95% Pu^{239}) of Pu-oxide kernels were achieved without particle failure. By comparison, experimental burn-ups of 79% of fertile and fissile content at temperatures of 1030-1240°C and fast fluences of 3.8E+21 n/cm^2 were reported in a study comparing German and U.S. fuel TRISO performance [23].

Transuranic TRISO fuel has been used in a series of conceptual designs of gas-cooled, fast, transmutation reactors (GCFTR) driven by a fusion neutron source [24, 25]. Both TRISO and BISO (bi-isotropic) fuel particles were examined, using SiC and zircalloy-4 fuel matrices, respectively. The series of GCFTR designs and the previous metal-fueled fast transmutation reactor designs are summarized by Stacey, et al. [18], and Stacey [17] has discussed how the development of the tokamak fusion neutron source would fit into the USDOE fusion program. The present work is based on the second of these designs [25]---GCFTR-2. Several fuel cycle scenarios are analyzed to explore how the GCFTR-2 design can achieve >90% burn-up of TRU, with an emphasis on the examining the possibility of doing so without reprocessing.

Section 2 describes the GCFTR-2 reactor design. An overview of fuel production is presented in section 3. Section 4 describes the computational methodology employed to model the design and simulate the fuel cycle. In section 5, the fuel cycle scenarios analyzed in this work are described. Section 6 discusses the results of the fuel cycle analyses in terms of transmutation performance. Section 7 presents a summary and conclusions of the work.

CHAPTER 2: REACTOR DESIGN

The reactor design used in this study and described in this section is based on the GCFTR-2 [25]. There are two differences between this reactor design and the GCFTR-2: 1) this design contains no lithium in the core while the GCFTR-2 has a small fraction of lithium in the core 2) the lithium content of the reflectors is different between this reactor and the GCFTR-2. Reactor dimensions and materials, however, are identical.

The reactor consists of a toroidal plasma chamber outboard of which is the reactor core (figure 1). Investing the plasma chamber is the first wall which is composed of ferritic HT9 steel (table 2). Both the first wall and reactor core are surrounded by the reflector that serves to conserve the neutrons generated by the various nuclear reactions and to breed tritium. The reflector consists of HT9 and a solid tritium breeder, Li_2O. The tritium produced in the reflector is removed via an on-line helium purge and is used to fuel the D-T fusion reaction. Surrounding the reflector is a shield composed of boron carbide and tungsten which served to protect the toroidal field coils from high-energy neutrons and gamma radiation, respectively. The vacuum vessel, composed of HT9, encases the shield and seals the reactor and plasma chamber from the outside environment. The magnets, depicted in figure 1 as gold loops, are based on ITER [25]. The core, first wall, magnets, central solenoid, reflector and shield are all cooled with helium.
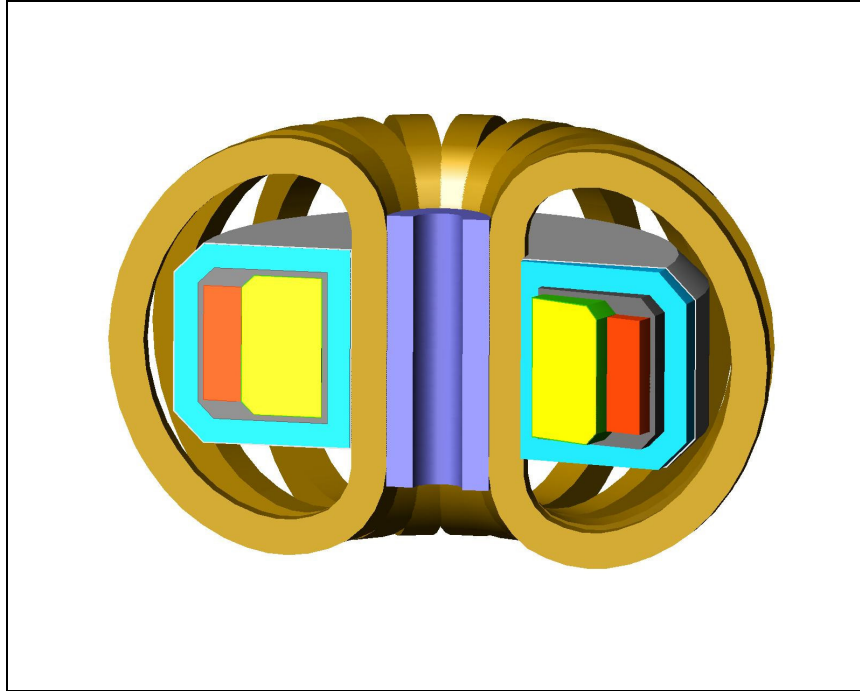
Figure 1. Schematic of the GCFTR-2.

Table 2. Reactor specifications.

Parameters and Materials	Values
Reactor Core	
Annular dimensions	R_{in} = 4.84 m, R_{out} = 5.96 m, H = 3 m
Fuel/He/structure v/o	59.5/30/10.5
Fuel element	TRISO particles in SiC matrix, pin d=1.34 cm
TRU coated particle diameter	660 μm
TRU-oxide fuel volume fraction	60%
TRU fuel mass	37 MT
Maximum k_{eff}	0.95
Clad/structural materials	Zircaloy-4/HT-9
Fission Power	3000 MW$_{th}$
Reflector	
HT9/He/Li$_2$O v/o	Various
Thickness	15 cm
Shield	
W/B4C/He v/o	40/40/20
Thickness	61 cm
Fusion Source	
EOC Pfus	200 MW

2.1. Core Design

As displayed in figures 2a and 2b, the core design consists of hexagonal fuel assemblies with a flat-to-flat distance of 36.625 cm containing fuel pins (631/assembly, 185,000 total) with a pin pitch of 1.417 cm and a diameter of 1.34 cm. The helium coolant cools the assemblies by flowing through the interstices between the pins. The pins themselves consist of a solid solution of TRISO particles embedded in a SiC matrix all of which is clad with zircalloy-4[1]. The cladding was chosen for its high melting point of 1845°C and its long history in industry. The SiC matrix was chosen for its compatibility with the TRISOs, negligible absorption cross-section and the extensive industry experience with this material. Though the use of such low-Z elements for the matrix would seem counter-intuitive for a fast reactor design, the volume fraction allocated to the matrix is small enough so that the neutron spectrum remains fast (figure 3).

---

[1] It may be possible to replace zircalloy-4 cladding with a SiC coating. Zircalloy-4 cladding was used in this analysis.
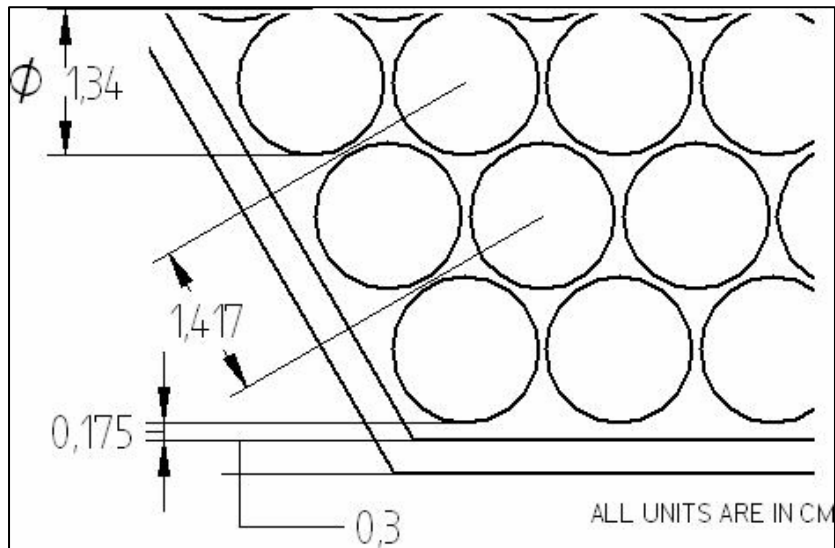
Figure 2a. Fuel pin and assembly layout – assembly close-up. [24]
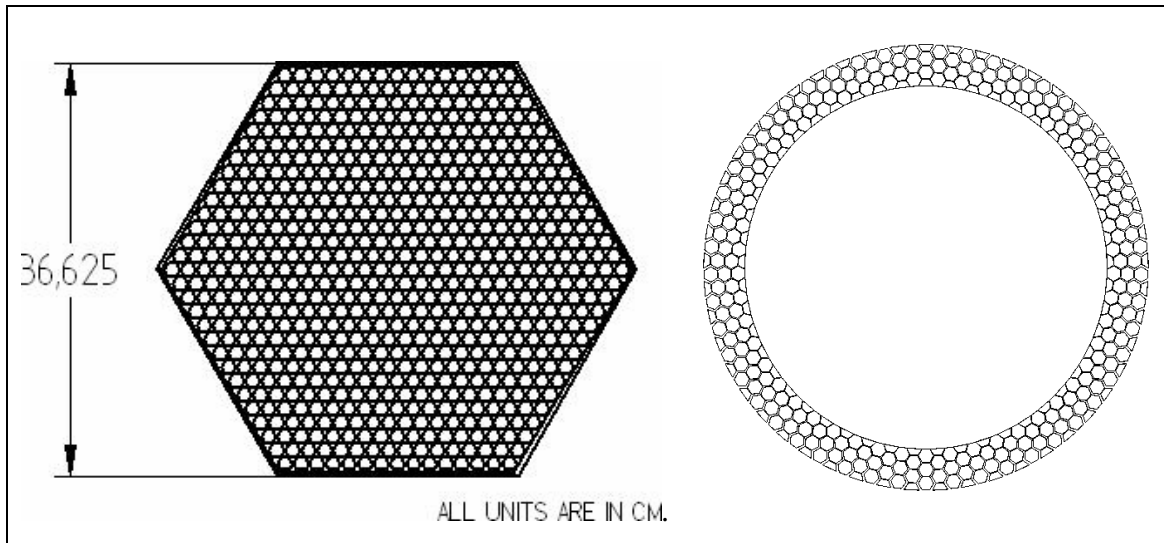
Figure 2b. Fuel pin and assembly layout – single assembly and whole core. [24]
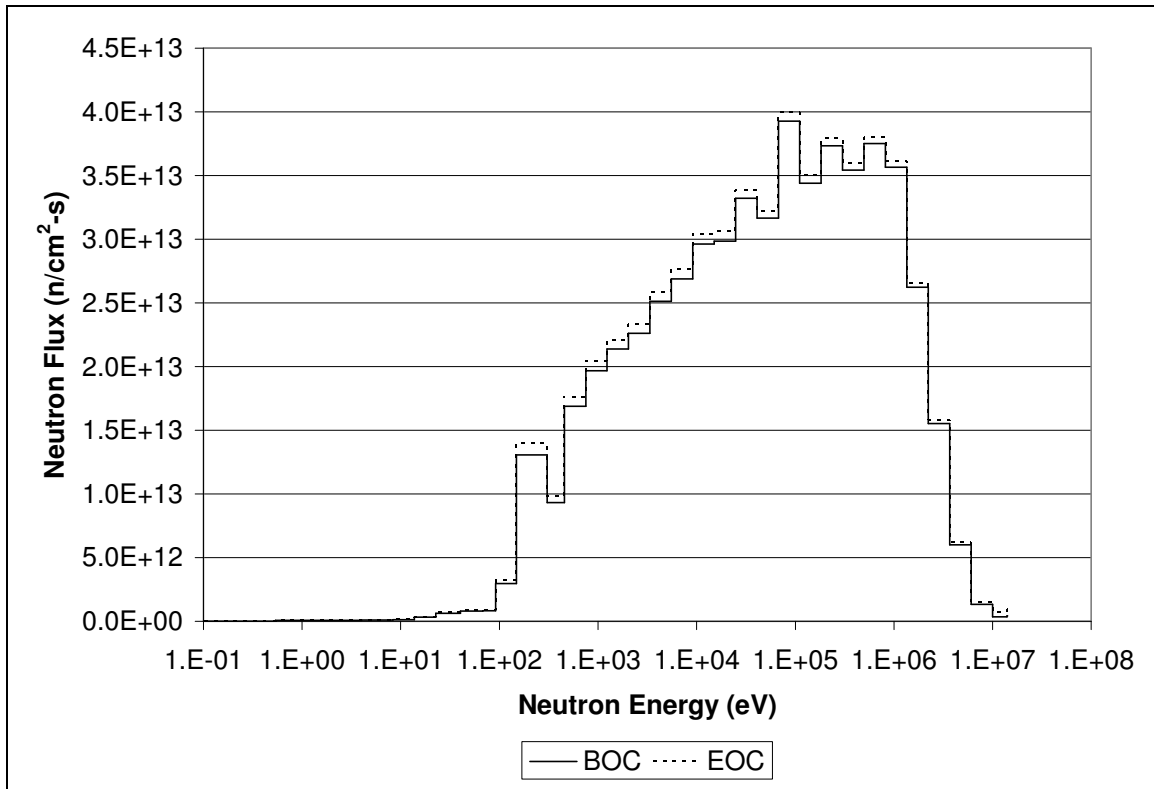
Figure 3. Representative flux spectrum.

The volume percents allocated to "fuel," structure and coolant of 59.5%, 10.5% and 30%, respectively, were developed by Stacey, et al. [25] to insure adequate heat removal of the core. "Fuel" refers to TRISO + SiC. The TRISO particles are micro-spheres, and there is a limit to what percentage of the volume of a given fuel element (pin minus clad) that they can occupy. The maximum occurs when the spheres touch each other with the minimal amount of space in between. This would correspond to about 64%, the balance taken up by the SiC matrix. Higher enrichments allow for longer burn times (thus greater availability), so the highest enrichment possible for the equilibrium fuel cycle was chosen for each scenario that was developed. A maximum of 60% was chosen because the theoretical limit of 64% would be difficult to consistently achieve in practice.

10

The core is divided into five annular regions as depicted in figure 4. The fuel in each region is called a "batch." Batches are moved from region to region in consecutive burn cycles and then discharged for recycling or storage.
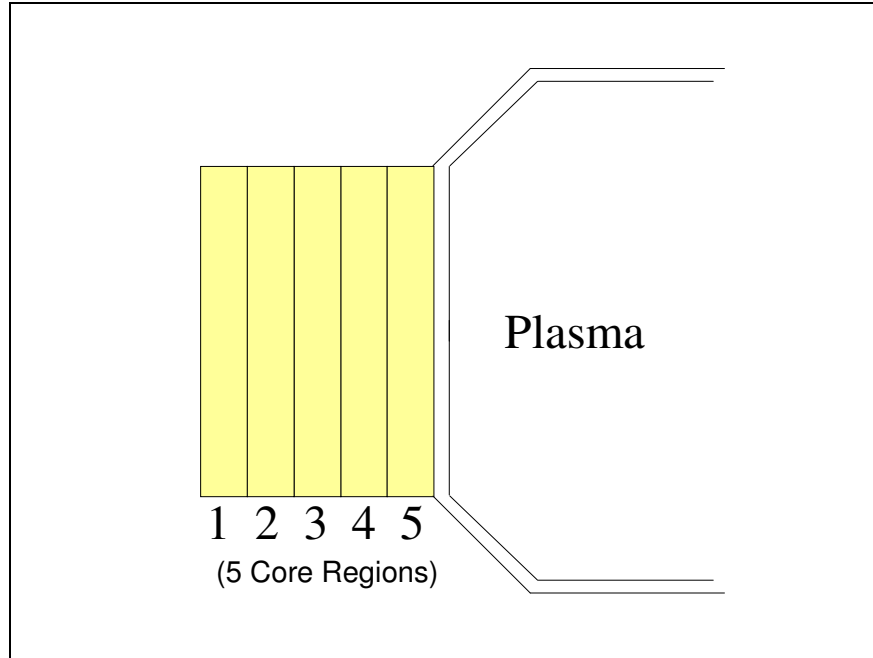
Figure 4. Reactor core.

The core operates sub-critically at a constant power of 3000 MWth. The fission neutron population must be held constant to maintain constant power. This is done by increasing the fusion neutron source over the burn cycle. Since the fissions deplete the TRUs and lower the value of k_{sub}, the source must be increased to compensate. The fusion neutron source is multiplied due to the fission of the TRUs according to equation 1.

$$N_{neutrons}^{total} = \frac{S}{1 - k_{sub}} = const. \tag{1}$$

The core also has a k_{eff} which is the Eigenvalue of the diffusion equation without the neutron source.

2.2. Tritium production

The tritium calculations for this design are different than those performed for the GCFTR-2 [25]. Here, tritium inventory is calculated over each cycle to ensure that a sufficient surplus is achieved at the end of a cycle, whereas the GCFTR-2 study calculated the BOC tritium breeding ratio (TBR) and used this to determine tritium self-sufficiency. The logic for lithium enrichments is taken from the GCFTR-2 study.

The fusion source generates neutrons via the D-T fusion reaction, $D + T \rightarrow {}^4He + n$. Deuterium is readily available in nature, but tritium must be produced via neutron capture in lithium for which the following reactions obtain:

$$ {}^6Li + n \rightarrow {}^4He + T \tag{2} $$

$$ {}^7Li + n \rightarrow {}^4He + T + n' \tag{3} $$

Tritium self-sufficiency is accomplished by placing a solid breeder, Li_2O, in the reflector regions surrounding the core. Referring to Appendix A, 30% enriched (in Li-6) Li_2O was placed in the inner reflector and 90% enriched Li_2O was placed in the central and outer reflectors. No Li_2O was used in the upper reflector. (Note that the lithium content in the reflector regions differ from that of the GCFTR-2 due to different computer models used to approximate the design.)

Different lithium enrichments were used in the inner reflector than in the central and outer reflectors in order to take advantage of the (n, α) cross sections of Li6 and Li7 (see Appendix B) which are larger in thermal and fast spectra, respectively. Since the inboard side is more likely to experience fast neutron flux from the fusion source that will have energies of about 14.1 MeV, the Li_2O in this part of the reflector is enriched in Li6 to 30%, while the outboard part of the reflector is enriched to 90%, as most of the neutrons here will

12

be slow relative to the inboard reflector because they originate from fission. (Fission neutrons typically have energies of 1-2 MeV, which are moderated down into the 10-100 keV range in the core, as shown in figure 3.)

The tritium inventory was calculated for a given equilibrium fuel cycle based on the assumption that the reaction rate varies linearly over a given burn cycle. Fusion and tritium reaction rates are calculated from fusion power and flux data provided by REBUS-3, respectively. The lithium content of the core was adjusted such that over an equilibrium cycle enough tritium was produced to sustain the fusion reaction. Enough surplus tritium also had to be produced to allow for a between-cycle down time of 90 days[2] and to provide enough fuel for some fraction of the next burn cycle. Since an on-line gas purge is used, it is not necessary to produce enough surplus tritium to fuel the fusion reaction for the whole of the next burn cycle, but only a part of it. Tritium from the previous burn cycle is needed only until the tritium is made available via the on-line gas system which may take a few weeks.

In the equations that follow, $N_T(t)$ is the amount of tritium available at time t. Ctime is the burn cycle time. The decay constant of tritium is denoted by λ for which the value of 8.1103E-02/years is used. T(t) and F(t) are the tritium production rate and the fusion rate at time t, respectively, and are calculated as shown in equations 4 and 5:

$$T(t) = \sum_{region} \sum_{l=Li6,Li7} \sum_{g=1}^{34} \phi_{g,region}^{t} \sigma_{g}^{l} N_{region}^{l,t} V_{region} \tag{4}$$

$$F(t) = \frac{P_{fus}^{t}(MW)}{17.6(MeV / fusion) * 1.6022E + 19(J / eV)} \tag{5}$$

The instantaneous rate of change of $N_T(t)$ is shown in equation 6:

---

[2] The default refueling down-time used in the REBUS-3 calculations was just 30 days. Ninety days was used as a conservative estimate in the event of some off-normal condition.

$$\frac{d\mathrm{N}_T(t)}{dt} = -F(t) + T(t) - \lambda \mathrm{N}_T(t) \tag{6}$$

Using a linear approximation for both the fusion rate and tritium production rate, we have the following:

$$\frac{d\mathrm{N}_T(t)}{dt} = -\left[F(boc) + \frac{(F(eoc) - F(boc)) * t}{Ctime} \right] + \left[T(boc) + \frac{(T(eoc) - T(boc)) * t}{Ctime} \right] - \lambda * \mathrm{N}_T(t) \tag{7}$$

Solving for N_T(eoc) we have:

$$\mathrm{N}_T(eoc) = \mathrm{N}_T(0) * e^{-Ctime*\lambda} + \frac{T(boc) - F(boc)}{\lambda} * (1 - e^{-Ctime*\lambda}) +$$
$$+ \frac{[T(eoc) - T(boc) + F(eoc) - F(boc)]}{\lambda^2 * Ctime} * (\lambda * Ctime - 1 + e^{-Ctime*\lambda}) \tag{8}$$

The tritium necessary at the start of a given fuel cycle must last until the tritium from the on-line gas purge system is ready for use. This amount is denoted $\mathrm{N}_T(0)$. The actual surplus tritium left at the beginning of a given fuel cycle is denoted $\mathrm{N}_T(0')$. $\mathrm{N}_T(0')$ is that amount that has been accumulated over the previous cycle and decayed for the "between-cycle down-time" of 90 days. This value must be $\geq \mathrm{N}_T(0)$ in order for tritium self-sufficiency to exist.

In the calculations to determine tritium self-sufficiency, a 90 day down-time was assumed and the amount of time into the next burn cycle for which the fusion reaction could be sustained using tritium from the previous cycle was calculated. In the results tables in the following sections, this time is called the "lead time" and must be greater than a week or so.

The equations used to calculate $\mathrm{N}_T(0)$ and $\mathrm{N}_T(0')$ are shown below in equations 9 and 10, respectively. The relationship that must obtain for tritium self-sufficiency is equation 11.

$$\mathrm{N}_T(0) = \left[F(boc) + \frac{(F(eoc) - F(boc)) * leadtime}{Ctime} \right] * leadtime \tag{9}$$

$$N_T(0') = N_T(eoc) * e^{-\lambda * \text{downtime}} \tag{10}$$

$$N_T(0') \geq N_T(0) \tag{11}$$

Tritium self-sufficiency was achieved for all scenarios except for scenario C. The results of these calculations are displayed in the tables of section 6.

CHAPTER 3: TRISO FUEL PARTICLE

A summary of the processing, fabrication and composition of the TRISO fuel particle designed in the GCFTR [24] and GCFTR-2 [25] studies and used for the present design is included in this section. The LWR SNF (see Appendix C) undergoes a four part DIDPA partitioning process to separate the TRUs from the SNF [25, 26]. Estimated recovery percentages for the TRUs using this process are 99.85% for Np and Pu and 99.97% for Am and Cm with negligible retention of lanthanides and uranium [25] which is modeled here as perfect separation of FPs, lanthanides and uranium from the TRUs and TRU recovery as per the aforementioned fractions. Subsequent to separation, the TRUs are oxidized in a calcination process, blended and homogenized [24] to form the TRISO kernel. After kernel creation, a Chemical Vapor Infiltration (CVI) process successively deposits the outer layers of the TRISO particle [25]. The resulting kernel composition is shown in table 3.

Table 3. TRISO kernel data.

Isotope	TRU composition (10^{24} atoms/cc)	Oxide form	Oxide Melting Point (^{o}C)	Oxide Density (g/cc)
NP237	1.06508E-03	$NP237O_2$	2510	11.10
PU238	3.04308E-04	$PU238_2O_3$	2085	10.50
PU239	1.31692E-02	$PU239_2O_3$	2085	10.50
PU240	5.17324E-03	$PU240_2O_3$	2085	10.50
PU241	9.39158E-04	$PU241_2O_3$	2085	10.50
PU242	1.12804E-03	$PU242_2O_3$	2085	10.50
PU244	3.82484E-08	$PU244_2O_3$	2085	10.50
AM241	2.22727E-03	$AM241_2O_3$	2190	11.77
AM242m	1.61267E-06	$AM242m_2O_3$	2190	11.77
AM243	2.46366E-04	$AM243_2O_3$	2190	11.77
CM242	4.22866E-09	$CM242_2O_3$	2225	11.85
CM243	4.27069E-07	$CM243_2O_3$	2225	11.85
CM244	2.77358E-05	$CM244_2O_3$	2225	11.85
CM245	2.98895E-06	$CM245_2O_3$	2225	11.85
CM246	2.36385E-07	$CM246_2O_3$	2225	11.85
CM247	2.38486E-09	$CM247_2O_3$	2225	11.85

Each TRISO particle is approximately $660\,\mu m$ in diameter and consists of a TRU-oxide kernel $300\,\mu m$ in diameter surrounded by: 1) a ZrC buffer region of $100\,\mu m$ thickness, 2) an inner pyrocarbon layer of $20\,\mu m$ thickness, 3) a SiC layer of $25\,\mu m$ thickness and 4) an outer pyrocarbon layer of $35\,\mu m$ thickness [25].

The buffer is 50% void which allows for the expansion of FP gases and free oxygen and serves as a shock-absorber for the recoiling FPs. Zirconium carbide was used rather than carbon because the Zr acts as an "oxygen getter" resulting in a reduced oxygen partial pressure on the inner pyrocarbon layer [24].

The inner pyrocarbon layer, while providing some structural support, is primarily a means to protect the SiC layer from contact with chemicals employed in the deposition of the buffer layer.

The primary structural support is the SiC layer, which can withstand a maximum pressure of 345 MPa [24]. Since internal gas pressure is 160 MPa at 90% FIMA (Fissions Initial heavy Metal Atom) and 180 MPa at 99% FIMA (at fuel centerline temperatures of 1690°C and 1510°C, respectively) [24], particle failure due solely to fission gas and oxygen pressure is unlikely.

CHAPTER 4: COMPUTATIONAL METHODOLOGY

Fuel cycle calculations were performed by the fuel cycle modeling and depletion code REBUS-3 [27]. Transport calculations were performed with TWODANT [28], a two-dimensional, discrete ordinates, flux distribution code using an S4 approximation. Region-dependent cross-sections were generated using MCC-2 [29] with 34 groups (table 4) using the ENDF-B/V cross-section library and BOC number densities[3] for each core material at the operating temperatures specified in table 5. The coolant temperature for a given region, where not specified, is 50K less than the temperature of the given region.

Table 4. Energy group boundaries.

Group	Upper Bound (eV)	Group	Upper Bound (eV)
1	14191000	18	5530.8
2	14009000	19	3354
3	10000000	20	2034
4	6065000	21	1234.1
5	3678000	22	748.5
6	2231300	23	453.9
7	1353000	24	304.32
8	820800	25	148.6
9	497870	26	91.66
10	301900	27	67.904
11	183100	28	40.16
12	111090	29	22.6
13	67370	30	13.709
14	40860	31	8.315
15	24788	32	4
16	15030	33	0.54
17	9118	34	0.414

---

[3] For the purpose of generating cross sections, fission product concentrations were approximated at 50% of their discharge density as indicated by the equilibrium TRU single-pass burn-up (i.e. an equilibrium cycle with a 20% single-pass burn-up would be modeled with a FP content corresponding to a 10% burn-up in all core regions).

Table 5. Material temperatures used for cross-section calculations.

Temperature (K)	Region
750	Core Fuel
660	Core Coolant
700	Core Structure
600	Shield
600	Reflector
600	Magnet
600	Central Solenoid
600	First Wall
600	Vacuum Vessel

The geometry of the reactor was modeled by REBUS-3 as described in Appendix A. It was modeled in "R-Z geometry" which means that it is expressed in terms of radial and axial dimensions relative to a central axis and reactor mid-plane. Only the upper half of the reactor was modeled to take advantage of its symmetry about the mid-plane. It is modeled as toroidally symmetric.

The core was divided into 25 regions (5 radial core regions, each with 5 axial subdivisions of equal height…see Appendix A). The widths of the 5 core regions were adjusted to equalize the volumes which allowed for a given batch to be moved from one core region to the next without a change in fuel density. The number densities were homogenized over each of the 25 regions.

Depletion was modeled only for the actinides. Fission products were modeled as lumps. Neither the fission products in the core nor the lithium in the reflectors were depleted.

Four different fuel shuffling schemes, or "paths," were used for the four scenarios (scenario A, B, C and D described in section 6) developed in this study (figure 5). The numbers below the core designate the core region, while the numbers in the core itself

indicate the sequence each batch follows through the core. Scenario A used all four paths. Scenarios B, C and D used "path 1" of scenario A.
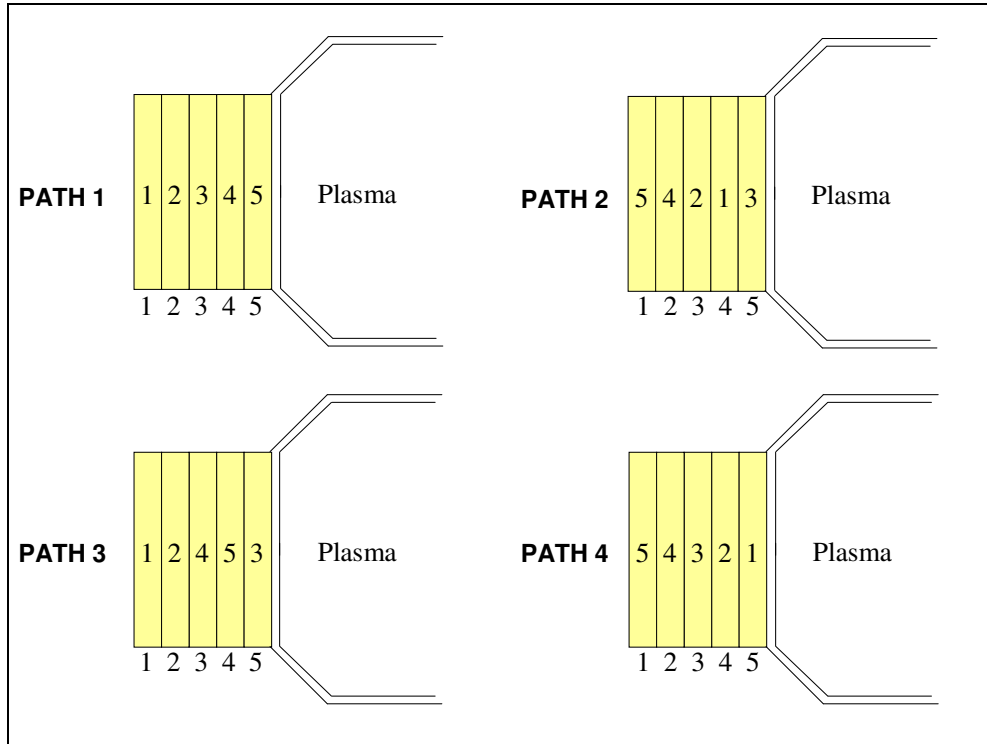
Figure 5. Fuel paths.

The fuel paths are directions for how fuel moves through the reactor in successive burn cycles. For example, a fresh batch of fuel in a 5-batch core may start in region 1 and move to region 2, then 3, then 4 and finally 5, and then it is discharged. This is "path 1" of figure 5. Another path is the reverse: a batch starts in region 5, then moves to 4, 3, 2 and finally 1, and then it is discharged. This is "path 4" of figure 5. Batches using "path 2" begin in region 4 and move to regions 3, then 5, then 2 and finally 1, and then the fuel is discharged. Batches using "path 3" follow the reverse sequence. They begin in region 1, then move to 2, 5, 3 and finally 4, and then they are discharged. Paths 2 and 3 arose from the observation that for a homogeneous core composition the magnitude of the flux is highest in

region 4, the penultimate flux occurs in region 3, then 5, 2 and 1 (see figure 6). Thus path 2 matches burn rank to flux rank. This was done to maximize the cycle time. The opposite of this, path 3, was used to minimize the power peaking.
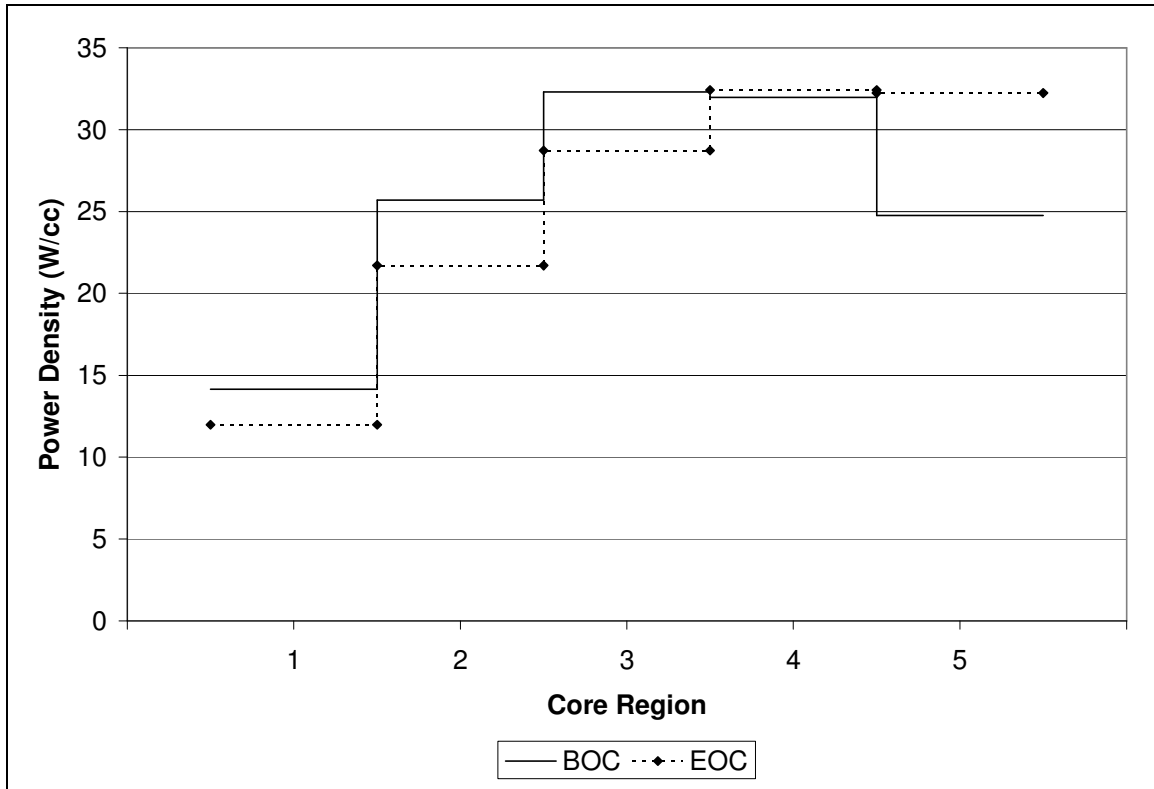
Figure 6. Power distribution for all-fresh core.

REBUS-3 models the fuel paths by specifying the sequence of core regions in which the fuel batches burn. It also models the between-cycle down-time during which the batches are moved to the next core region in the sequence and fresh fuel is added. A down-time of 30 days was used based on the GCFTR-2.

After discharge, the fuel is not immediately processed because it is highly radioactive. It is cooled for a time to allow the radioactivity to decrease. A cooling time of 730.5 days (based on the GCFTR-2) was modeled.

All fuel cycle calculations were for "equilibrium" fuel cycles. Equilibrium fuel cycle refers to a steady-state fuel cycle where the composition of the fuel charged to and discharged from the core, as well as the core composition itself, have all become constant due to a large number of executions of the fuel cycle. All core parameters have become steady-state. This is in contradistinction to a start-up core which will necessarily have different core enrichment and performance parameters from cycle to cycle which will change as new core batches are introduced and old batches removed.

To illustrate the concept of the equilibrium fuel cycle we take the example of path 1 whose burn history is depicted in figure 7. The 5 regions of the core each contain different batches of fuel at start-up (image A) with enrichments suitable to achieve the desired k_{eff}^{BOC}. The initial enrichments for each of the core batches are chosen by REBUS-3 to approximate core performance after a great number of burn cycles. The number "0" indicates that these batches are fresh, i.e. they have not yet been irradiated. This core is irradiated for the specified cycle time. At EOC, every batch has been irradiated once as shown in image B.

Figure 7. Burn sequence for path 1.

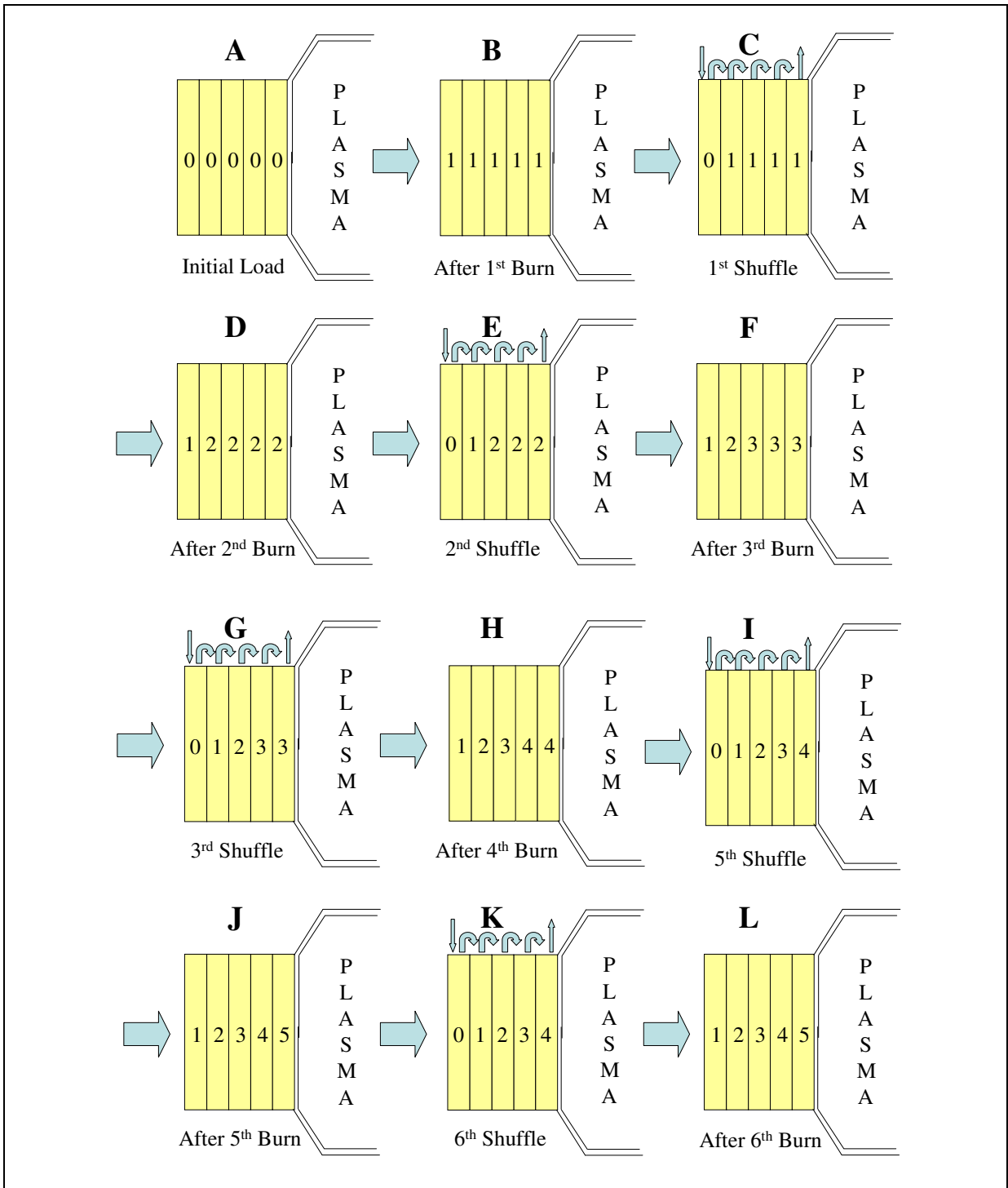Image C depicts both the fuel "shuffling" that occurs after the first burn and the resulting core loading. Each batch moves inward to the adjacent core region. The innermost

batch will be removed from the core and go to a reprocessing facility while the four once-burned batches will move like this: the batch in region 1 will go to region 2, 2 to 3, 3 to 4 and 4 to 5. Fresh fuel is placed in the outermost region, region 1, with a higher enrichment than the batches of the first burn in order to compensate for the reactivity losses of the once-burned batches so that the k_{eff}^{BOC} can be achieved again.

This new core configuration is burned for another cycle time. At EOC the batches have been burned as shown in image D. The fuel moves again (image E) in the same pattern sending another batch from region 5 to the reprocessing facility and bringing another fresh batch into region 1 with a new, higher enrichment.

After the third burn, the EOC core is image F, after the fourth, image H and after the fifth, image J, each one with a higher new batch enrichment to offset the reactivity losses of all the previous burns so to achieve the k_{eff}^{BOC}. The last EOC pattern, 1 2 3 4 5, will continue for all successive burn cycles. The new batch will continue to change enrichments until the change is so small that successive new batches are essentially identical. Discharge and intermediate compositions will also settle down to a steady-state at which time the equilibrium fuel cycle has been reached.

The "fixed-enrichment search" and "enrichment search" options of REBUS-3 were used to arrive at equilibrium fuel cycles for the four scenarios developed in this study.

"Enrichment search" was the method of performing equilibrium fuel cycle calculation using REBUS-3 used for scenario A and scenario D. In an enrichment search, the fuel loading is searched for that is necessary to achieve the desired equilibrium fuel cycle parameters of thermal power, k_{eff}^{BOC} and cycle time. REBUS-3 performs an iterative search until it converges on the equilibrium fuel cycle within the specified k_{eff}^{BOC} tolerance and

reports the fraction of TRU the user has allocated to the core that is required to meet the chosen performance characteristics. Based on these results, the user will increase or decrease the fuel volume fraction, as the case may be, and run another case until the desired enrichment is achieved. A tolerance of < 1% of TRU enrichment was used.

"Fixed-enrichment search" was used to determine the equilibrium fuel cycles for scenarios B and C. The equilibrium fuel cycle is found for the given fuel cycle parameters of thermal power, fresh feed composition and cycle time.

CHAPTER 5: DEEP BURN TRANSMUTATION FUEL CYCLE SCENARIOS

The primary objective is to achieve > 90% burn-up of the TRU fuel. The secondary objective is to do this without having to reprocess the TRISO particles. How these objectives can be met depends primarily on the limits placed on k_{eff}^{BOC} and P_{fusion}^{EOC}. The four scenarios in this study explore the effect of changing the restrictions placed on k_{eff}^{BOC} and P_{fusion}^{EOC} with respect to achieving the primary and secondary design objectives.

In scenario A, the k_{eff}^{BOC} is restricted to 0.95, the P_{fusion}^{EOC} is restricted to < 200 MW and reprocessing is performed. In scenario B, the k_{eff}^{BOC} is allowed to be < 0.95, the P_{fusion}^{EOC} is restricted to < 200 MW and reprocessing is performed. The reprocessing of scenarios A and B is with the following assumptions: (1) constant TRU isotopic composition during irradiation and (2) perfect extraction of the TRUs during reprocessing. In scenario C, the k_{eff}^{BOC} is allowed to be < 0.95, no restrictions are placed on P_{fusion}^{EOC} and a single-pass fuel cycle is used. In scenario D, the k_{eff}^{BOC} is allowed to be < 0.95, the P_{fusion}^{EOC} is restricted to < 200 MW and reprocessing is not performed.

A summary of the scenarios presented is given in table 6.

Table 6. Summary of scenarios.

Scenario	Description
Scenario A	Fuel reprocessed, BOC k-eff = 0.95, EOC Pfus < 200 MW
Scenario B	Fuel reprocessed, BOC k-eff < 0.95, EOC Pfus < 200 MW
Scenario C	Fuel not reprocessed, BOC k-eff < 0.95, no restriction on EOC Pfus
Scenario D	Fuel recycled w/o reprocessing, BOC k-eff < 0.95, EOC Pfus < 200 MW

The requirement that the core must have a k_{eff}^{BOC} of 0.95 (chosen to increase the margin to prompt criticality) is a restriction on core reactivity (equation 12). This is effectively a restriction on the TRU mass in the core because the reactivity depends on the TRU mass. A deeper burn will result in less TRU mass and lower reactivity. Longer burn times will result in deeper burn, so the k_{eff}^{BOC} restriction is also a restriction on cycle time (equation 14).

Consider the 5-batch core of this design. Fuel will debut in one core region, burn there, and then move in succession to the other core regions. Thus after a batch has been burned once, it will still be in the core for the next four burn cycles where it will contribute to the reactivity of the whole core. The more it is burned, the lower this contribution will be[4]. Since the degree of its burn depends on how long it has been burned, the k_{eff}^{BOC} restriction becomes a restriction on cycle time.

When it has burned once in every region (5 total burns), it will leave the core and be cooled for a time before it is reprocessed or placed in storage and a new batch will be placed in the region in which the discharged batch debuted. This new batch will compensate for the reactivity losses incurred by the batches remaining in the core, but only up to a point, because only so much fuel will fit in the fuel pins (the maximum practical packing fraction limit of 60%). This is a continuous process, so that at EOC, one 5-burned batch is discharged and one fresh batch is inserted into the core.

Once the cycle time is found such that the new batch must have the 60% packing fraction to achieve $k_{eff}^{BOC} = 0.95$, the amount of burn-up that can be achieved in a single pass

---

[4] It should also be noted that no fertile material is present in the fuel, which would also serve to compensate for reactivity losses because it would generate new fissile material via neutron capture and decay.

through the core has been maximized. Increasing the cycle time any more will increase the single pass burn-up but will also necessarily decrease the k_{eff}^{BOC}. Thus a restriction on k_{eff}^{BOC} is effectively a limit on the cycle time and thus on the cumulative burn-up a given batch will experience in a single pass through the core.

The requirement that the core must have a $P_{fusion}^{EOC} < 200$ MW (P_{fusion}^{EOC} limit of GCFTR-2), like the k_{eff}^{BOC} restriction, is also a restriction on core reactivity (equation 13) and thus limits the burn-up by limiting cycle time (equation 14). The fusion neutron source supplements the neutron population of the reactor core such that the fission power of 3000 MWth can be constantly maintained. As the burn-up increases over a burn cycle, the fusion power must be increased. Thus a larger burn-up will require a larger fusion power, and the 200 MW limit on source strength becomes a limit on the burn-up and cycle time.

$$k_{eff}^{BOC} \Rightarrow M_{TRU}^{core,BOC} \tag{12}$$

$$P_{fus}^{EOC} \Rightarrow k_{eff}^{EOC} \Rightarrow M_{TRU}^{core,EOC} \tag{13}$$

$$k_{eff}^{BOC} - k_{eff}^{EOC} \Rightarrow M_{TRU}^{core,BOC} - M_{TRU}^{core,EOC} = \Delta M_{TRU}^{core} \Rightarrow cycle\ length \tag{14}$$

It was found that the $k_{eff}^{BOC} = 0.95$ restriction resulted in $P_{fusion}^{EOC} \approx 95\,MW$, automatically satisfying the $P_{fusion}^{EOC} < 200$ MW restriction.

These restrictions on core reactivity do not prevent the primary objective from being achieved as long as 1) recycling is possible or 2) 90% burn is achieved in a single pass through the core (5-batch burn). If the single-pass burn-up is < 90%, recycling is necessary.

It is not possible to achieve 90% burn in a single pass while maintaining a k_{eff}^{BOC} of 0.95 because the deep burn lowers the core TRU mass too much. For the same reason, it is

not possible to achieve 90% burn in a single pass if k_{eff}^{BOC} is allowed to be < 0.95 while

maintaining the $P_{fusion}^{EOC} < 200$ MW. Thus it is necessary to consider recycling. Since these of

k_{eff}^{BOC} and P_{fusion}^{EOC} restrictions are limits on core reactivity, they determine what *type* of

recycling is possible, i.e. (1) recycling with reprocessing or (2) recycling without

reprocessing. The restrictions determine the type of recycling because the two types differ in

the reactivity of the recycle streams. Type (1) recycling has a more reactive recycle stream

than type (2) since type (2) will contain FPs that act as parasitic absorbers.

In type (1) recycling (figure 8), the TRISO fuel discharged from the reactor is taken

apart and the kernels are separated into FPs and unburned TRU. The FPs are sent to a

HLWR and the unburned TRUs join the mixture of TRUs from processing of LWR SNF.

This combination of fresh TRUs from LWR SNF and unburned TRUs from irradiated

TRISOs is used to form new TRISO particles that will be formed into fuel pins and burned

again in the reactor.
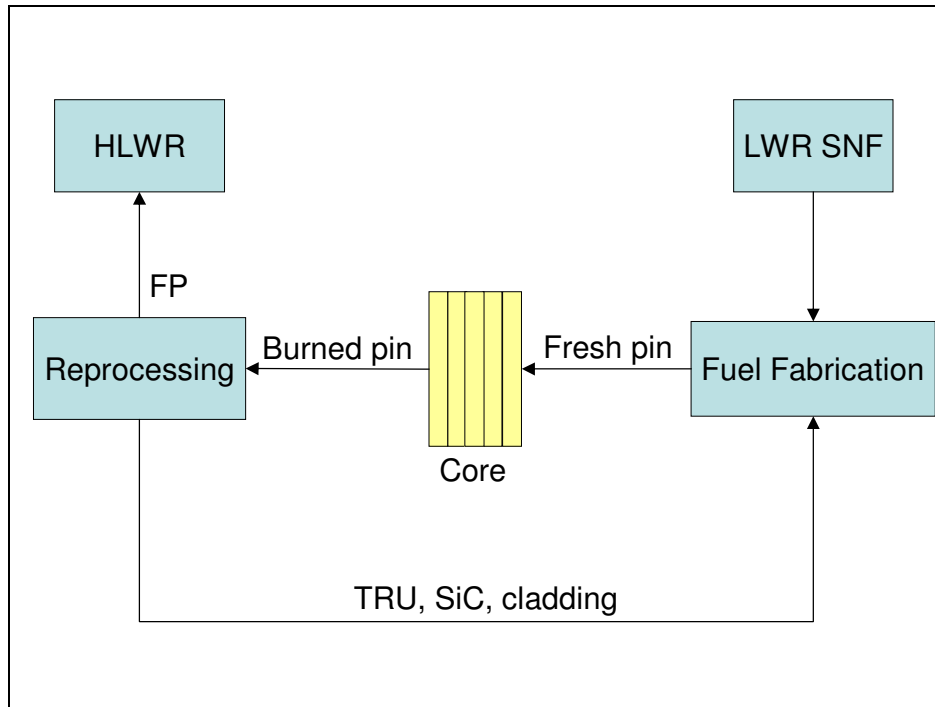
Figure 8. Type 1 recycling (TRISOs reprocessed).

In type (2) recycling (figure 9), the fuel discharged from the reactor is not

reprocessed, thus the FPs that accumulate during irradiation will remain with the fuel. The

burned fuel is mixed with newly fabricated fuel. The mixture of burned pins and new pins is

burned in the reactor.
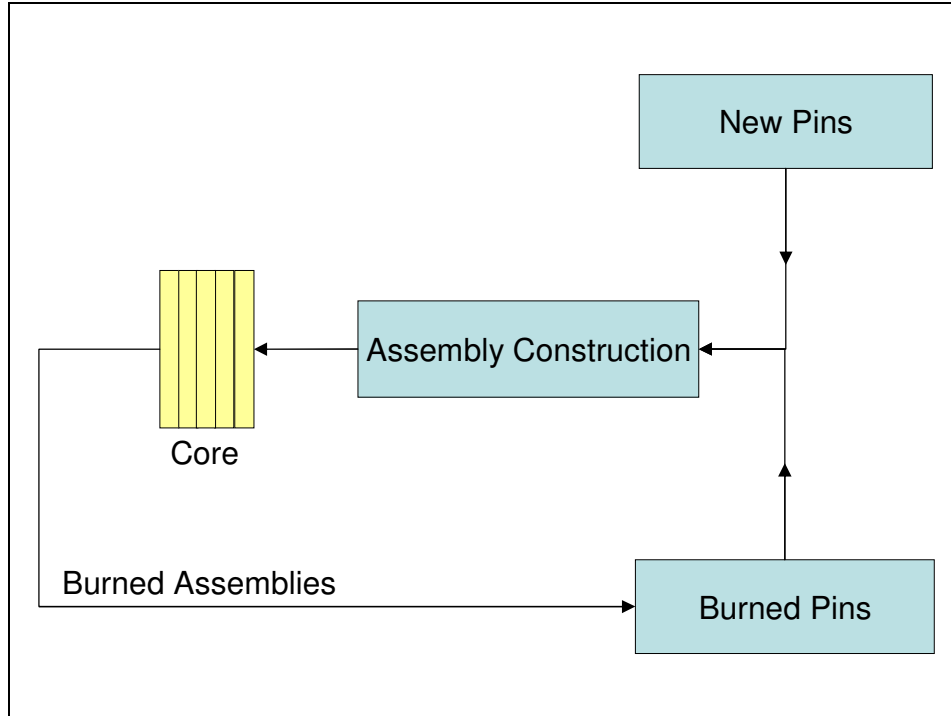
Figure 9. Type 2 recycling (TRISOs not reprocessed).

In order to achieve the secondary objective, only type (2) can be used. This was found to be impossible with $k_{eff}^{BOC} = 0.95$ and $P_{fusion}^{EOC} < 200$ MW and very inefficient with $k_{eff}^{BOC} < 0.95$ and $P_{fusion}^{EOC} < 200$ MW, thus type (1) recycling was also considered.

Scenario A was the first fuel cycle explored in this study. It is a recycling fuel cycle with reprocessing in which both the k_{eff}^{BOC} and P_{fusion}^{EOC} restrictions are enforced. Four versions of scenario A were evaluated, each with a different fuel path, with the purpose of evaluating burn-up as a function of fuel path.

Scenario B arose from the observation that for scenario A, the P_{fusion}^{EOC} was approximately 95 MW, far short of the 200 MW limit. The more restrictive $k_{eff}^{BOC} = 0.95$ restriction was removed to increase the burn-up per 5-batch burn by maximizing the cycle

time and thus reduce the number of passes required to achieve 90% burn. Scenario B, like scenario A, is a recycling case with reprocessing.

In scenario C, both the $k_{eff}^{BOC} = 0.95$ constraint was relaxed and the fusion power was increased to the level necessary to achieve 90% burn in just one pass (no recycle necessary).

In scenario D, recycling without reprocessing was explored to achieve the secondary objective. It is similar to scenario B in that the k_{eff}^{BOC} was allowed to be < 0.95 while the P_{fusion}^{EOC} was restricted to < 200 MW. It is different from the other three scenarios in that the input feed is a mixture of two feed streams of different composition: (1) low-reactivity recycled fuel from previous reactor discharges and (2) high reactivity fresh fuel from LWR SNF.

Fuel that is discharged from the reactor at the end of a burn cycle is sent back through the reactor continuously, completely destroying the TRU content of the fuel. Since reprocessing is not employed, the FPs are retained and build up over the duration of the burn and constitute a parasitic absorber. The changing composition of the TRU fuel also tends toward a less reactive isotopic composition as irradiation continues (see section VI.F.). Thus the recycled fuel becomes increasingly less reactive as irradiation continues. This makes it necessary to supplement the core loading of each batch with fresh feed, i.e. brand new TRISOs that have been created from LWR SNF.

The two feed streams are mixed such that as much of the recycle stream as possible is used in the new core charge. When this new batch has itself burned 5 times, i.e. completed a single pass, it will be discharged to the recycle stream where it mixes homogeneously with the rest of the discharged fuel. This recycle feed is combined with more fresh fuel for another charge.

Scenario D was evaluated at a cycle time of 330 days to maximize the fraction of the feed stream composed of recycled fuel. Three hundred thirty days maximizes the recycle fraction because it imposes the least restrictive requirements on reactivity within the design constraints. It should be recalled from the discussion on the relationship between k_{eff}^{BOC} and cycle time that the longer the cycle time, the lower the equilibrium core reactivity. Minimizing the cycle time at 330 days will thus minimize the required equilibrium core reactivity and maximize the amount of recycled fuel in the reactor feed.

The recycle stream will consist of fuel of a variety of burn-ups since it will be a combination of the discharge of every fuel cycle. Ideally, the recycled TRISOs would be removed from the fuel cycle once 90% burn-up of the TRUs is reached and would be sent to a HLWR. In the recycling fuel cycle modeled here, however, the fuel never leaves the fuel cycle, which means the recycle stream will be less reactive than in the ideal case. So scenario D constitutes a conservative estimate to a recycling fuel cycle in which fuel is removed at 90% burn.

Design constraints in addition to k_{eff}^{BOC} and P_{fusion}^{EOC} were enforced/desired as shown in table 7 below. Power peaking was limited to below 2 for safety reasons. The packing fraction was limited to 60%. The tritium inventory produced during a given cycle was designed to last for a between-cycle down-time of at least 90 days to ensure an adequate supply. It was also desired that the cycle time exceed 330 days to ensure reasonable availability.

Table 7. Design constraints/goals.

Parameter	Units	Value/Range
Cycle Length	days	>= 330
EOC Pfus	MW	< 200
BOC k-eff		<= 0.95
Power Peaking		< 2
Between-cycle Tritium	days	90
TRISO Packing Fraction	%	<= 60%

CHAPTER 6: TRANSMUTATION PERFORMANCE

The terminology used in the output tables is defined in section 6.1. The results of scenarios A, B, C and D are discussed in section 6.2., 6.3., 6.4. and 6.5., respectively. Specific characteristics of the four fuel paths of scenario A are discussed in sections 6.2.1 – 6.2.4.

6.1.   Discussion of terminology used in output data

Some terms used in the data table require explanation.   The "Burn rate/batch/residence" is intended to evaluate each path with regard to the rate at which it destroys TRUs from the initial emplacement in the reactor to its extraction at the end of the 5th burn cycle. It takes into account the between-cycle down-time of 30 days.

The "SNF disposal rate" refers to the mass of SNF whose TRU content has been destroyed in the reactor in one FPY. Since the TRU content of the reference SNF is about 1%, and each path results in the destruction of 1.12 MT/FPY, the disposal rates of all the fuel cycles are about 100 MT/FPY.

The "LWR support ratio" refers to the ratio of TRU destroyed by a given reactor to TRU produced by a 1000 MWe LWR in a FPY. Since a typical 1000 MWe LWR will produce about 360 kg of TRU/FPY [14] as compared to 1.12 MT destroyed by a GCFTR-2, the support ratio is 3 for all paths.

The "TRU burn/residence" was calculated as a simple mass balance of the TRU isotopes present in the fresh fuel over an equilibrium cycle (isotopes of table 3).

"Tritium Inter-cycle down-time" indicates the decay time, in days, between cycles accounted for in the tritium production requirements. The actual between-cycle down-time

modeled for the equilibrium calculations was 30 days, the longer time of 90 days being a conservative estimate to account for off-normal conditions.

"Tritium lead-time" refers to the amount of time, in days, into the next equilibrium burn cycle that tritium would be available from the previous cycle. The minimum value is a few weeks.

"Core passes for 90% burn" values were calculated based on the single-pass burn-up derived from the REBUS-3 output. REBUS-3 calculates the equilibrium compositions of the reactor charge and discharge. The mass decrease of the TRUs present in the "fresh" TRISOs (TRUs listed in table 3) determines the single-pass burn or "TRU burn/residence." As fuel is reprocessed or recycled and sent back through the reactor, it is assumed to experience the same TRU burn/residence. Based on this accumulated burn-up, the number of passes required to achieve >90% burn-up is calculated.

For example, if the charge TRU loading is 100 MT, and the TRU burn/residence is 20%, the discharge (five-times-burned fuel) batch will contain 80 MT of TRU. For the next pass, 20 MT will be used as make-up. After the next pass, the 80 MT recycled and the 20 MT make-up TRU will both have been reduced by 20% to 64 MT and 16 MT, respectively. The "core passes for 90% burn" indicates the number of such core passes required to reduce the original 100 MT to < 10 MT.

6.2. Scenario A

The results (table 8) indicate that the primary objective is achieved by all paths and complete destruction of the TRUs will be achieved at a rate of 1.1 MT of TRU/FPY. However, the 330 day cycle time goal was not achieved for any path. Since the fuel in this scenario is the most optimistic with respect to recycled feed reactivity and it still cannot

37

attain 330 days, type 2 recycling certainly cannot be achieved with this scenario. Fuel recycled without reprocessing will contain FPs, which act as parasitic absorbers, and will have a less reactive composition. Less reactive fuel, in turn, will result in lower cycle times. For this reason type 2 recycling cases with $k_{eff}^{BOC} = 0.95$ could not be achieved for this design.

Table 8. Scenario A (BOC k-eff = 0.95, EOC Pfus < 200 MW) results.

Parameter	Units	Path 1	Path 2	Path 3	Path 4
Cycle Length	days	280	305	240	260
5 Batch Residence	years	3.83	4.18	3.29	3.56
Packing Fraction	%	60%	60%	60%	60%
BOC k_{eff}		0.951	0.949	0.950	0.951
EOC k_{eff}		0.924	0.919	0.928	0.927
BOC P_{fus}	MW	38.7	39.3	39.7	38.5
EOC P_{fus}	MW	91.3	94.7	82.4	90.5
Lithium Fraction in Reflector[1]	%	4.07%	4.50%	3.65%	4.35%
Tritium Burned/Cycle	kg	2.74	3.07	2.21	2.53
Tritium Produced/Cycle	kg	2.83	3.17	2.28	2.64
Tritium Inter-cycle Down-time	days	90	90	90	90
Tritium Lead Time	days	180	185	162	222
BOC Power Peaking		1.70	1.83	1.63	1.73
EOC Power Peaking		1.52	1.71	1.47	1.62
TRU BOC Load	MT	35.3	34.6	35.3	34.9
TRU EOC Load	MT	34.4	33.7	34.6	34.1
TRU Burn/Batch/Residence	MT	0.86	0.93	0.73	0.79
TRU Burned/Core/Year	MT/FPY	1.12	1.12	1.11	1.12
TRU Burn/Residence	%	11.6%	12.7%	10.0%	10.8%
Burn Rate/Batch/Residence[2]	kg/day	0.553	0.558	0.542	0.548
LWR Support Ratio[3]		3	3	3	3
SNF Disposed per year	MT/FPY	100	100	100	100
Average Cycle Flux	n/cm^2-s	5.62E+14	5.66E+14	5.59E+14	5.60E+14
Average Cycle Fast Flux[4]	n/cm^2-s	2.33E+14	2.34E+14	2.31E+14	2.32E+14
Fluence/Residence	n/cm^2	6.80E+22	7.45E+22	5.79E+22	6.29E+22
Fast Fluence/Residence	n/cm^2	2.81E+22	3.08E+22	2.40E+22	2.61E+22
Core Passes for 90% Burn		19	17	22	21
Total Residence for 90% Burn	years	73	71	72	75
Fluence at 90% Burn	n/cm^2	1.29E+24	1.27E+24	1.27E+24	1.32E+24
Fast Fluence at 90% Burn	n/cm^2	5.35E+23	5.24E+23	5.28E+23	5.48E+23

[1]Only applies to inner, outer and central reflectors. The upper reflector contains no lithium.
[2]Includes a 30-day down-time between cycles.
[3]Assuming 360kg TRU produced/FPY [14].
[4]Fast Flux is >0.11MeV.

Single-pass burn-up ranged from 10% to 12.7%. The burn rate was essentially the same among the four paths, varying by less than 3%.

The $P_{fusion}^{EOC} < 200$ MW requirement is satisfied as a consequence of the k_{eff}^{BOC} constraint. This is due to the fact that the cycle times necessary to achieve $k_{eff}^{BOC} = 0.95$ all corresponded to P_{fusion}^{EOC} values of 90 – 95 MW.

The average cycle fluxes and fast fluxes, though not equal, are all very close to one another. Since the cycle times vary from path to path, however, the fluence also varies, with the highest seen in the paths with the highest cycle times. The P_{fusion}^{EOC} also follows this trend since longer cycle times make for deeper burn requiring greater compensation from the neutron source to maintain the power level. Thus the ranking of P_{fusion}^{EOC}, from highest to lowest, corresponds to the ranking of cycle times, from highest to lowest. In consequence of this, the tritium consumption follows the same trend since tritium is the fuel for the fusion neutron source.

All cases operated with power profiles sufficient to maintain the power peaking below the design goal of 2.

The neutron flux energy distribution varied only slightly among the four paths, so path 1 was taken to be representative of them all. As shown in figure 10, almost the entire flux is contained in the range from 100 eV to 10 MeV.
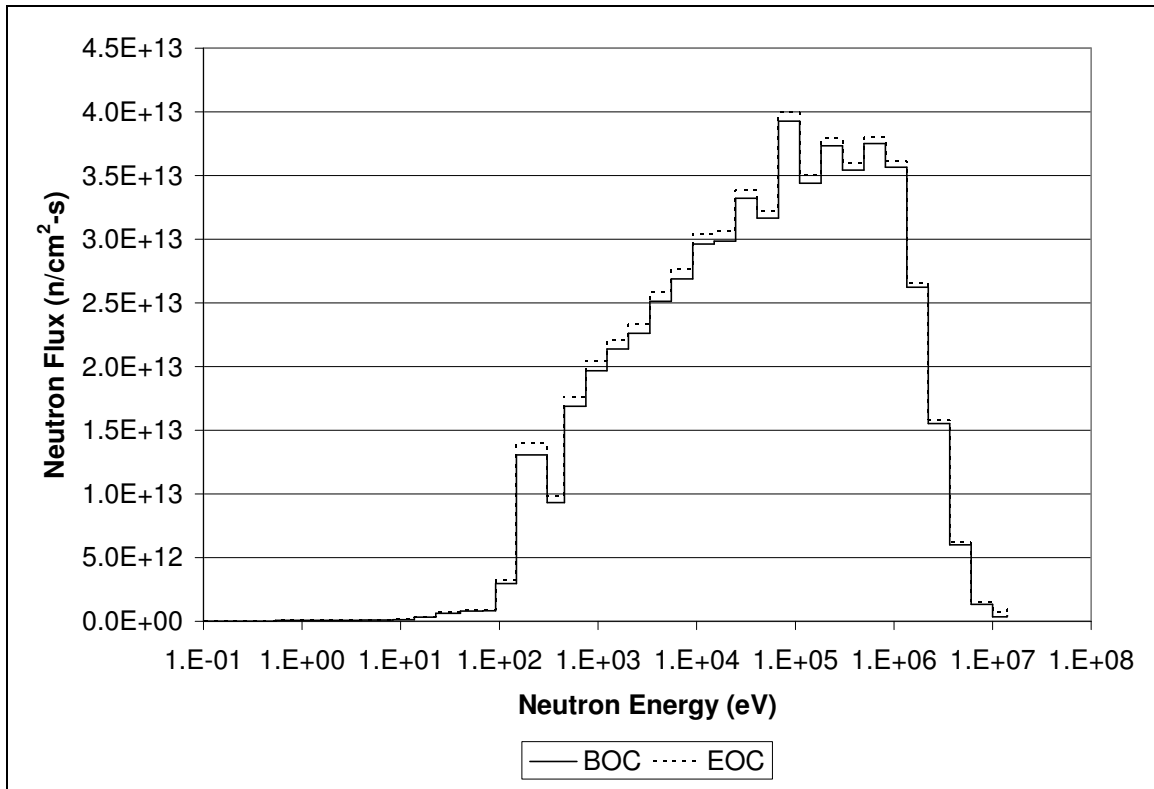
Figure 10. Scenario A flux spectrum.

6.2.1. Path 1

Path 1 consists of a simple out-to-in shuffle pattern. The fuel cycle time was limited to 280 days as a consequence of the k_{eff}^{BOC} restriction of 0.95 (see section 5 discussion). A greater cycle time could have been achieved were it possible to increase the TRU volume fraction of the core, but this is not possible considering that the TRISO packing fraction is already maximal at 60%. This 280 day cycle time results in an 11.6% burn-up of the initial TRU content per pass through the reactor.

The average BOC and EOC axially-averaged radial power distributions are shown in figure 11 for path 1. The low power densities are a consequence of REBUS-3 performing the power calculations over the whole volume of the specified sub-region as opposed to just over

the volume of the fuel. Thus the figures are meant to show relative power distributions rather than absolute power levels.
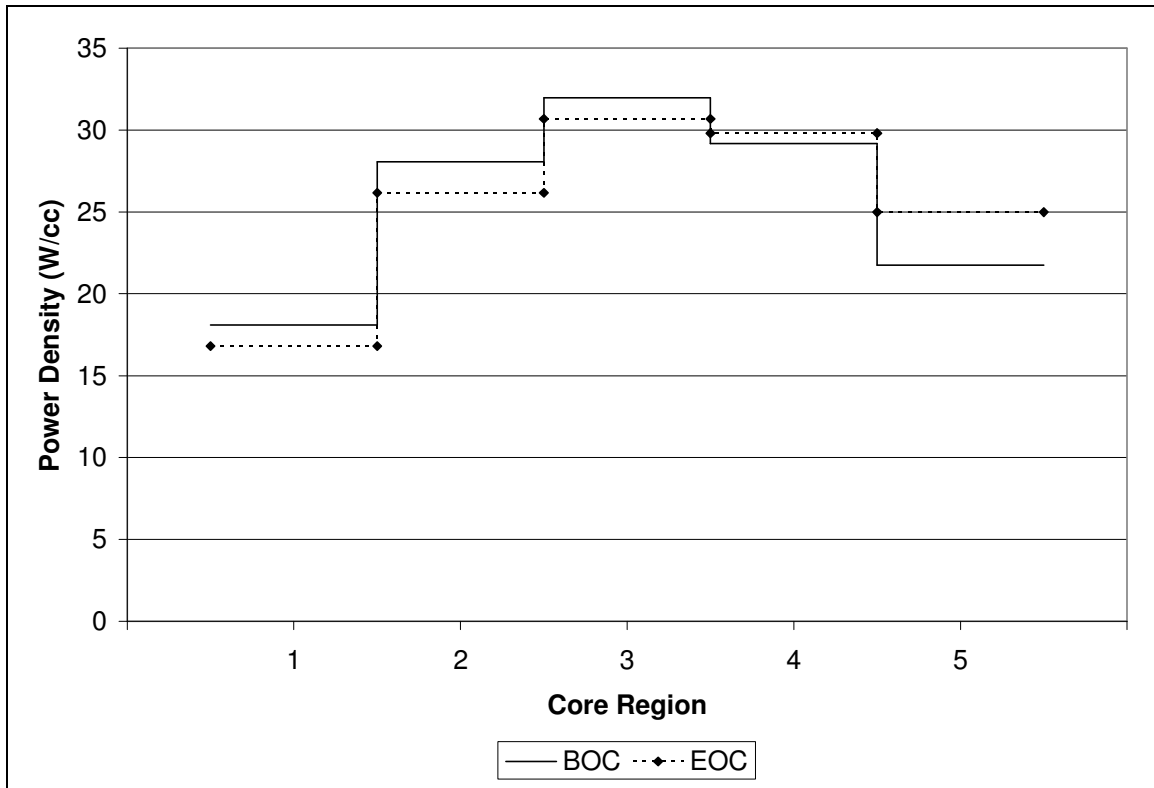
Figure 11. Path 1 power distribution.

6.2.2. Path 2

In path 2, the fuel follows a path from highest flux region to lowest flux region in an effort to increase the cycle time such that a greater availability could be achieved (target > 330 days). The intent of this case is to maximize cycle time by keeping the most reactive fuel in the regions that naturally have the highest flux. In a typical reactor, this would be similar to a cosine peaking in the center and symmetric in the radial direction. This reactor, however, has a source on the in-board side, shifting the peak towards the source so that the highest flux region occurs in region 4 (see figure 6, pg. 17). The power distribution shown is

for a core with all 5 regions loaded with identical, fresh fuel. The substantial shift of power (and thus flux) towards the plasma is distinct, both at BOC and even more so at EOC.

Averaging BOC and EOC, we can rank the core regions highest average power to lowest average power as follows: 4, 3, 5, 2 and 1. The fuel for path 1 follows this same sequence debuting in the reactor in region 4, moving through 3, 5 and 2 and finally burning in region 1. As one would expect, this case has the highest power peaking (but is still under the design limit of 2). It also achieves the highest cycle time (305 days) as was the intent, though still shy of the 330 day goal.
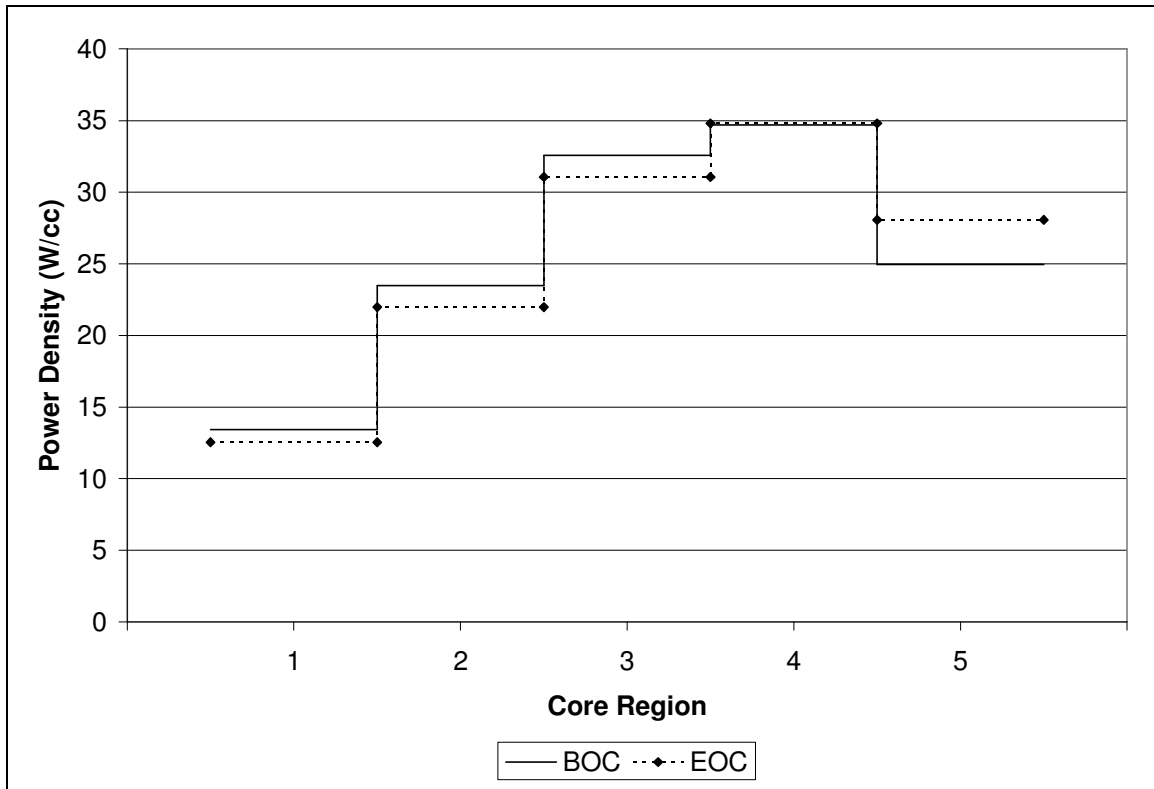
Figure 12. Path 2 power distribution.

6.2.3. Path 3

In path 3, the fuel follows a path from lowest flux region to highest flux region (the converse of path 2) in an effort to flatten the power profile and minimize the peaking. It has the shortest cycle time (240 days), highest k_{eff}^{EOC}, lowest tritium burn, lowest lithium volume fraction in the reflectors and lowest P_{fusion}^{EOC}. It also has the lowest power peaking making it the safest of the four paths.
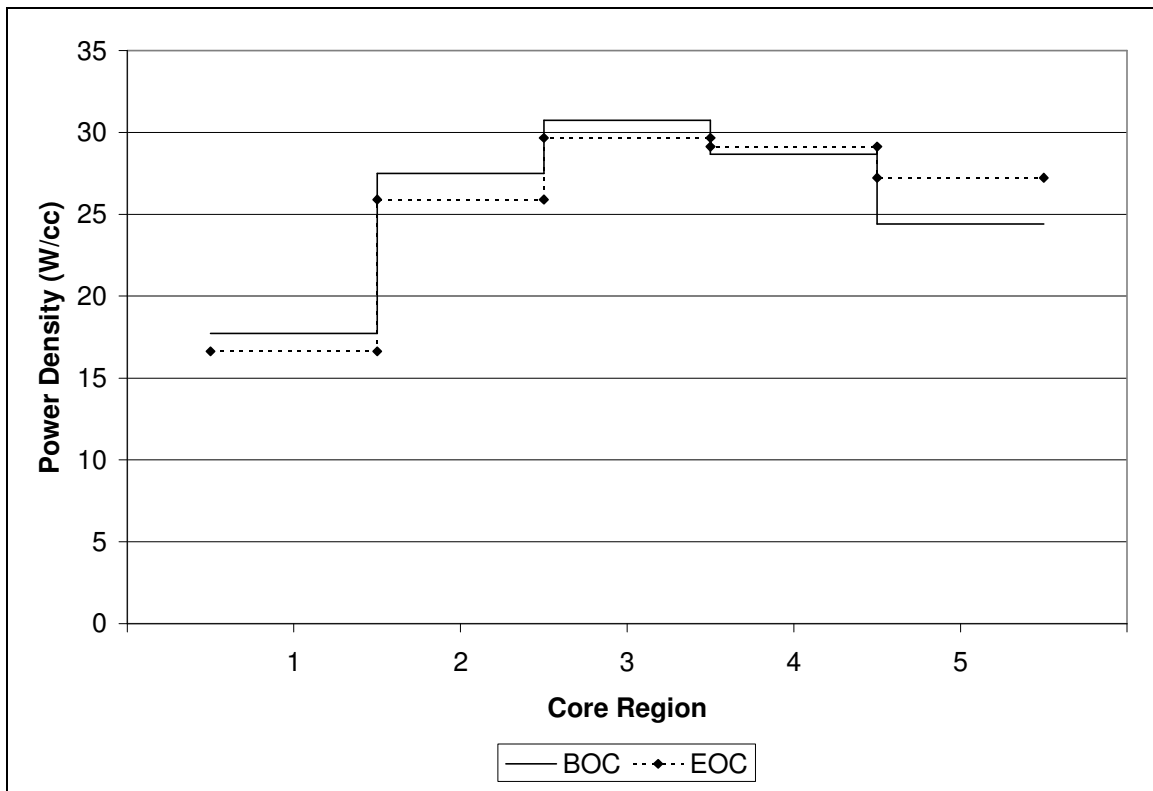
Figure 13. Path 3 power distribution.

6.2.4. Path 4

Path 4 is the converse of path 1. Path 4 has a slightly lower BOC core loading and higher power peaking relative to path 1 due to the proximity of fresh fuel to the flux peak.
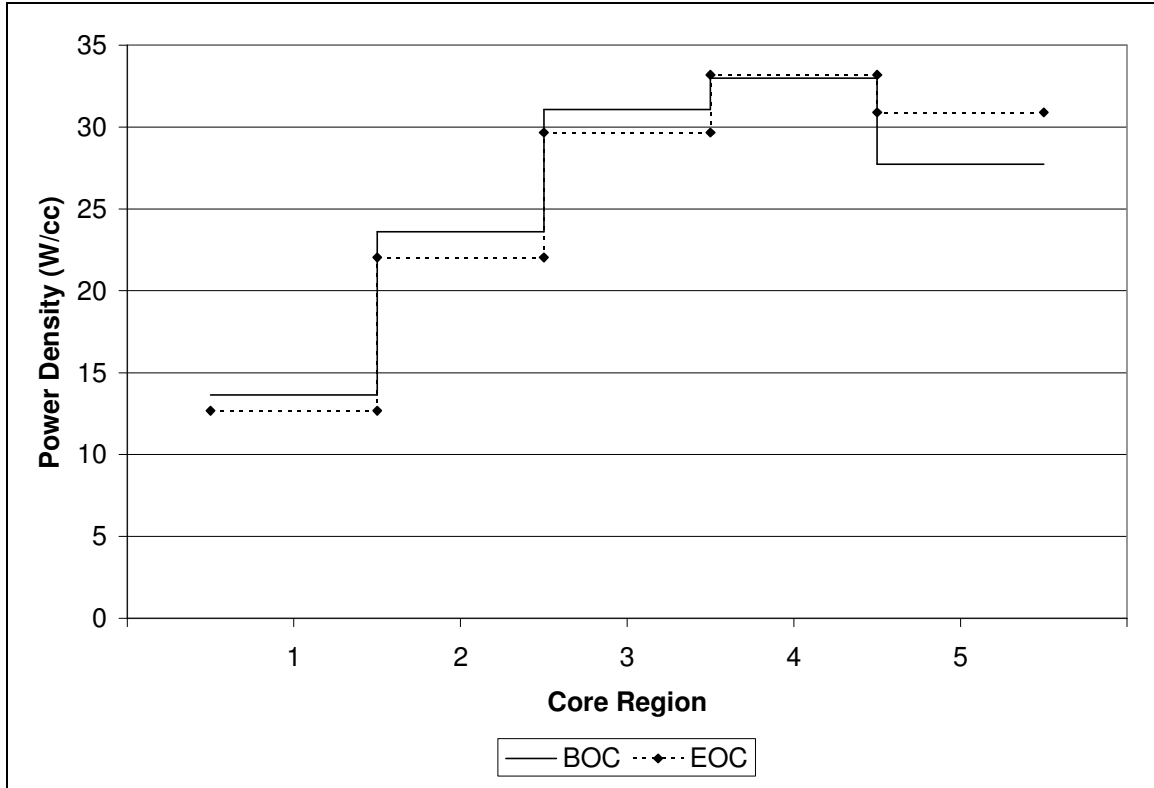
Figure 14. Path 4 power distribution.

6.3. Scenario B

See table 9 for the results of this fuel cycle. The k_{eff}^{BOC} was 0.857 and EOC was 0.823. The P_{fusion}^{EOC} was 199 MW. The larger fusion power relative to scenario A results in a much larger requirement for the tritium inventory and reflector lithium volume fraction. As was expected, loosening the k_{eff}^{BOC} constraint resulted in a longer fuel cycle (376 versus 280) for the chosen fuel path achieving the availability goal of > 330 day cycle time. The longer cycle time results in a larger single-pass burn-up (15.3% was achieved versus 11.6% achieved by path 1 of scenario A) but still much less than 90%. The TRU destruction rate is 1.13 MT/FPY.

The flux spectrum (figure 15) is almost identical to scenario A except for a slightly more energetic spectrum and a slightly larger flux, particularly at EOC. This is due to the

45

larger burn-up caused by a longer cycle time which necessitates a larger flux from the neutron source. This increases the fraction of the core neutron population composed of the more energetic fusion neutrons.

Table 9. Scenario B (BOC k-eff < 0.95, EOC Pfus = 200 MW) results.

Parameter	Units	Values
Cycle Length	days	376
5 Batch Residence	years	5.15
Packing Fraction	%	60%
BOC keff		0.936
EOC keff		0.930
BOC Pfus	MW	122.1
EOC Pfus	MW	199.1
Lithium Fraction in Reflector	%	28.00%
Tritium Burned/Cycle	kg	9.02
Tritium Produced/Cycle	kg	9.34
Tritium Inter-cycle Down-time	days	90
Tritium Lead Time	days	200
BOC Power Peaking		1.73
EOC Power Peaking		1.53
TRU BOC Load	MT	34.9
TRU EOC Load	MT	33.8
TRU Burn/Batch/Residence	MT	1.13
TRU Burned/Core/Year	MT/FPY	1.10
TRU Burn/Residence	%	15.3%
Burn Rate/Batch/Residence	kg/day	0.556
LWR Support Ratio		3
SNF Disposed per year	MT/FPY	98
Average Cycle Flux	n/cm^2-s	5.78E+14
Average Cycle Fast Flux	n/cm^2-s	2.42E+14
Fluence/Residence	n/cm^2	9.39E+22
Fast Fluence/Residence	n/cm^2	3.94E+22
Core Passes for 90% Burn		14
Total Residence for 90% Burn	years	72
Fluence at 90% Burn	n/cm^2	1.31E+24
Fast Fluence at 90% Burn	n/cm^2	5.51E+23
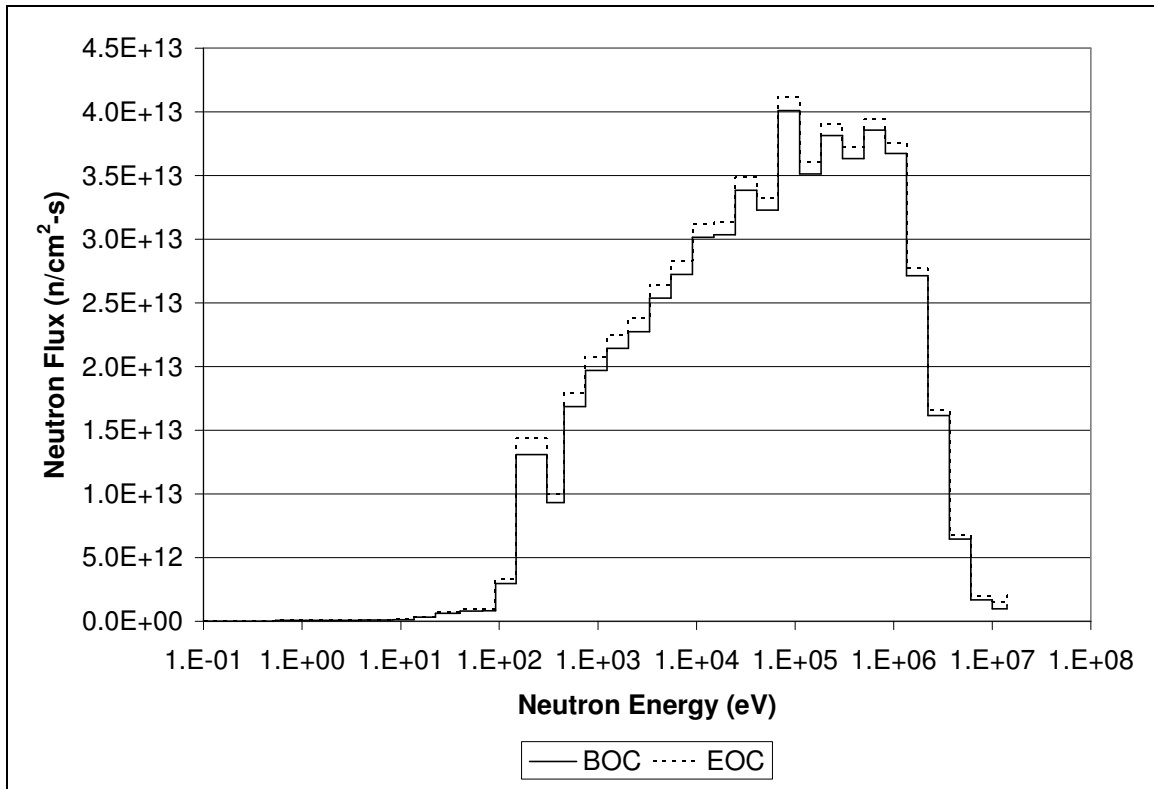
Figure 15. Scenario B (BOC k-eff < 0.95, EOC Pfus = 200 MW) flux spectrum.

6.4. Scenario C

See table 10 for the results. The single-pass equilibrium burn was 90.0% with a cycle time of 3000 days. Ninety percent burn would be achieved after 41 years of irradiation. The fusion power necessary to achieve this burn-up was 1803 MW at BOC and 3366 at EOC. The fast fluence at 90% is 6.45E+23 n/cm^2. Tritium self-sufficiency was nearly achieved with 76.3% of the required tritium produced. This required the entire volume of all of the reflector regions to be composed of Li$_2$O, including the upper reflector.

The flux distribution is depicted in figure 16. It indicates a much larger average core flux, particularly at EOC. The average core flux and average core fast flux are double that of the other three scenarios. This is due to the very high burn-up of this core which requires a much larger fusion power level to maintain the fission power level.

47

As a consequence of the high lithium concentration in the reflector and the larger core flux the exothermic tritium reactions contribute a much larger amount of the reactor power than the other scenarios. As a result, less TRUs need to be fissioned to maintain the power level, so the TRU destruction rate (0.81 MT/FPY) is lower than the other scenarios. The fraction of the total power that comes from the core is 81% at BOC and 67% at EOC, the balance coming primarily from the reflectors. For the other scenarios, the TRU destruction rate is 1.12 MT/FPY and ~97% of the reactor power is generated in the core with little variation from BOC to EOC.

The large demands placed on the fusion neutron source indicates that near-term deployment of such a reactor is not feasible and that reprocessing and recycling scenarios are the only means to 90% burn of the TRU fuel at the present time.

Table 10. Scenario C (single-pass, BOC k-eff < 0.95, no restrictions on EOC Pfus) results.

Parameter	Units	Values
Cycle Length	days	3000
5 Batch Residence	years	41.07
Packing Fraction	%	60%
BOC keff		0.383
EOC keff		0.127
BOC Pfus	MW	1803
EOC Pfus	MW	3366
Lithium Fraction in Reflector	%	100%
Tritium Burned/Cycle	kg	975
Tritium Produced/Cycle	kg	756
Tritium Inter-cycle Down-time	days	-
Tritium Lead Time	days	-
BOC Power Peaking		1.49
EOC Power Peaking		1.34
TRU BOC Load	MT	24.2
TRU EOC Load	MT	17.9
TRU Burn/Batch/Residence	MT	6.65
TRU Burned/Core/Year	MT/FPY	0.81
TRU Burn/Residence	%	90.0%
Burn Rate/Batch/Residence	kg/day	0.439
LWR Support Ratio		2
SNF Disposed per year	MT/FPY	73
Average Cycle Flux	n/cm^2-s	1.17E+15
Average Cycle Fast Flux	n/cm^2-s	4.97E+14
Fluence/Residence	n/cm^2	1.52E+24
Fast Fluence/Residence	n/cm^2	6.45E+23
Core Passes for 90% Burn		1
Total Residence for 90% Burn	years	41
Fluence at 90% Burn	n/cm^2	1.52E+24
Fast Fluence at 90% Burn	n/cm^2	6.45E+23
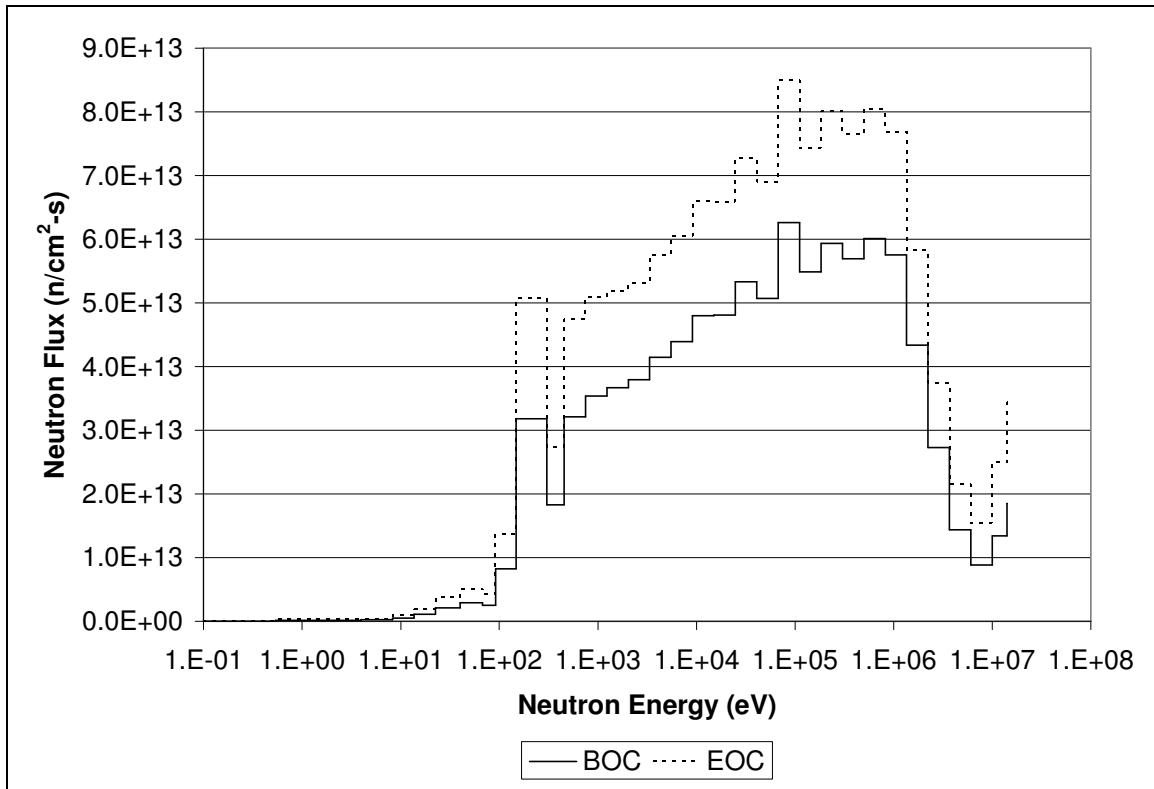
Figure 16. Scenario C (single-pass, BOC k-eff < 0.95, no restrictions on EOC Pfus) flux spectrum.

6.5. Scenario D

See table 11 for the results. Scenario D is an equilibrium fuel cycle with the maximum amount of fuel that can be recycled without reprocessing to achieve 90% burn-up in a burn cycle with a 330 day length, $k_{eff}^{BOC} < 0.95$, and $P_{fusion}^{EOC} < 200$ MW. Scenario D was the only scenario to meet both the primary (< 90% burn-up) and secondary (without reprocessing) design objectives as well as all of the design constraints (table 7, pg. 27) besides $k_{eff}^{BOC} = 0.95$. It was found that the equilibrium fuel cycle had a k_{eff}^{BOC} of 0.860 and an P_{fusion}^{EOC} of 188 MW. The TRU destruction rate of 1.11 MT/FPY and the LWR support ratio of 3 were the same as scenarios A and B. This was achieved by recycling only a small amount of burned TRU fuel with a large amount of fresh TRU. The recycled feed fraction was 6.2%

50

(by mass). This is not a very large number, but should be regarded as a lower bound considering that the computational model is a conservative estimate of the case in which TRISOs are removed after they achieve 90% burn.

The flux spectrum (figure 17) is essentially identical to scenario B.

A larger core and a more precise fuel cycle model in which TRISOs were removed from the fuel cycle at 90% burn would both serve to increase the recycled fuel fraction.

Table 11. Scenario D (recycling, BOC k-eff < 0.95, EOC Pfus < 200 MW) results.

Parameter	Units	Values
Cycle Length	days	330
5 Batch Residence	years	4.52
Packing Fraction	%	60%
Recycled Feed Fraction	%	6.2%
Fresh Feed Fraction	%	93.8%
BOC keff		0.860
EOC keff		0.827
BOC Pfus	MW	120.0
EOC Pfus	MW	187.5
Lithium Fraction in Reflector	%	25.00%
Tritium Burned/Cycle	kg	7.61
Tritium Produced/Cycle	kg	7.82
Tritium Inter-cycle Down- time	days	90
Tritium Lead Time	days	162
BOC Power Peaking		1.73
EOC Power Peaking		1.54
TRU BOC Load	MT	34.9
TRU EOC Load	MT	33.9
TRU Burn/Batch/Residence	MT	1.00
TRU Burned/Core/Year	MT/FPY	1.11
TRU Burn/Residence	%	13.7%
Burn Rate/Batch/Residence	kg/day	0.556
LWR Support Ratio		3
SNF Disposed per year	MT/FPY	99
Average Cycle Flux	n/cm2-s	5.76E+14
Average Cycle Fast Flux	n/cm2-s	2.42E+14
Fluence/Residence	n/cm2	8.22E+22
Fast Fluence/Residence	n/cm^2	3.45E+22
Core Passes for 90% Burn		16
Total Residence for 90% Burn	years	72
Fluence at 90% Burn	n/cm^2	1.31E+24
Fast Fluence at 90% Burn	n/cm^2	5.52E+23
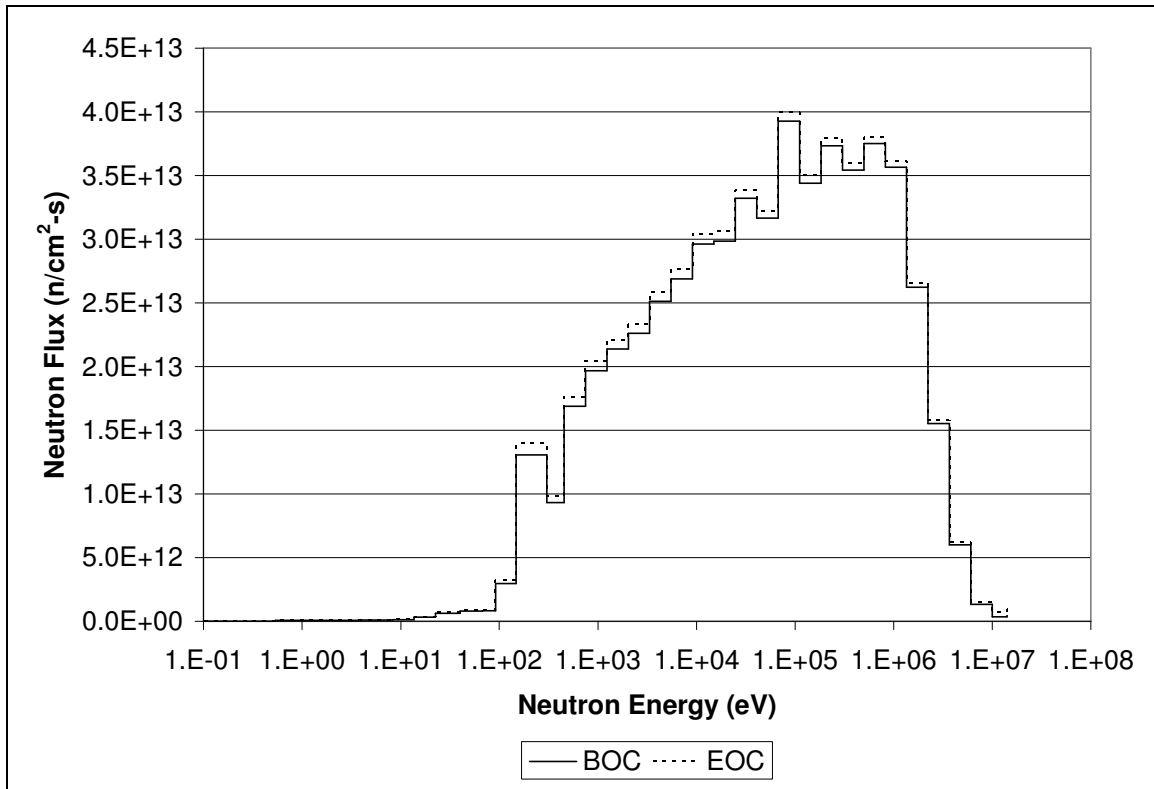
Figure 17. Scenario D (recycling without reprocessing, BOC k-eff < 0.95, EOC Pfus < 200 MW) flux spectrum.

6.6.   Isotopic Composition During Irradiation

The relative isotopic distribution of the TRU fuel was calculated at several equally-spaced time steps during irradiation to evaluate the reasonableness of the assumption made for the reprocessing cases of constant isotopic distribution during irradiation. The results are shown in figure 18. Isotopes not shown (Am243, Cm244, Pu240, Cm245, Pu241) each account for less than 1% for the duration of the burn and are omitted.

Far from being constant, the isotopic distribution changes significantly as irradiation proceeds. The first assumption used for the reprocessing approximations of scenarios A and B is thus incorrect. The predominant change in the distribution is the relative reduction of Pu239 and the relative increase of Pu241 and Pu242. Plutonium-239 has a smaller capture-to-fission ratio than either Pu241 or Pu242 by a factor of 2 – 3 in a fast spectrum indicating

53

that as the burn proceeds, the isotopic mixture is increasingly less reactive. Curium-244 also

increases from less than 1% to over 10% of the isotopic mixture and has a fast capture-to-

fission ratio comparable to that of Pu242. These changes also have to be weighed by the

depletion in TRU isotopes, because as burn proceeds, the contribution of a given sample of

previously-burned TRU will diminish. The net effect, however, is clearly towards less

reactivity than in the constant-isotopic-distribution assumption.

Though it is clear that the composition does not remain constant, further work is

necessary to quantify the impact of the effect of changing composition on reactor

performance and is beyond the scope of this study.
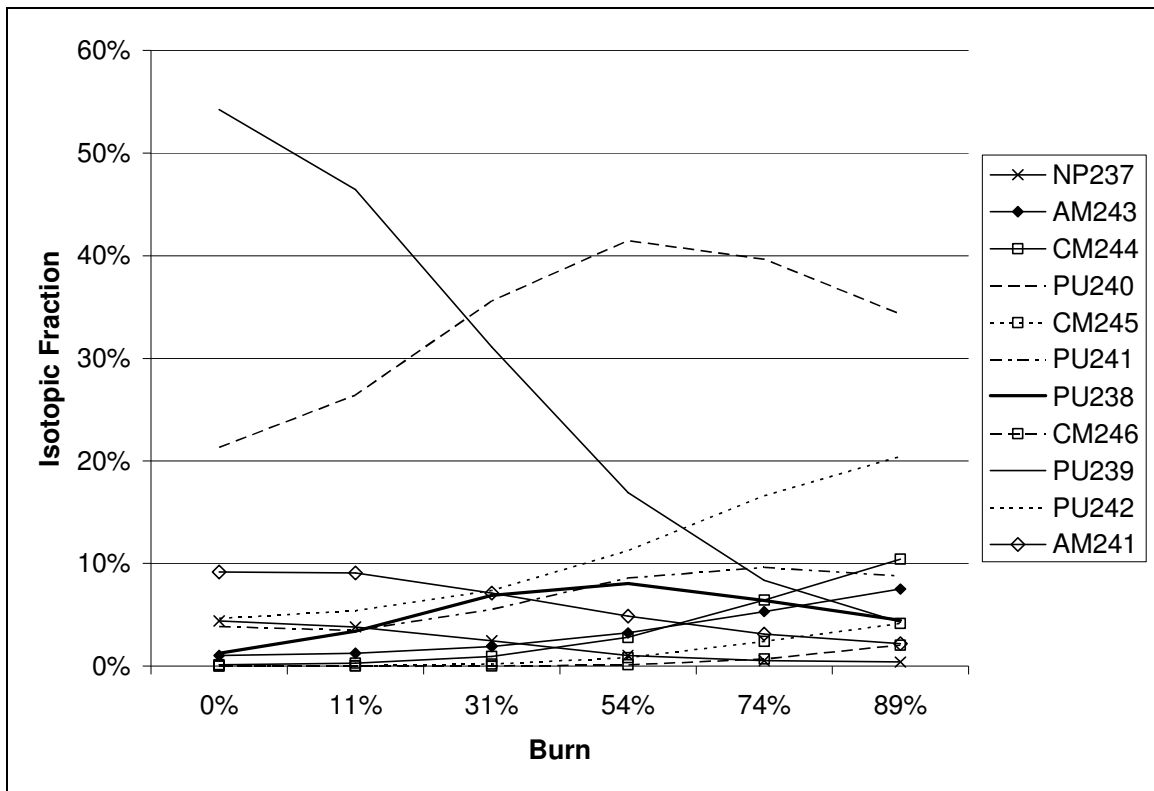
Figure 18. Isotopic distribution trends.

6.7.   Radiation Damage Limits to TRISO Particles

McEachern [29] indicates that fast fluences on the order of 4-8E21 n/cm^2 are limiting for TRISO particles in a fast spectrum – a value exceeded by even the lowest burn-up case of this study (10.0%) which saw a single-pass fast fluence of 2.40+E24 n/cm^2. However, this fluence limit is for the nominal TRISO particle designed for use in a thermal spectrum reactor. In the GCFTR-2 design the conventional TRISO design for thermal reactors has been modified by reducing the kernel and enlarging the buffer region in anticipation of fast fluence limitations. Thus TRISO failure due to radiation damage is as yet an unresolved issue for this design.

CHAPTER 7: SUMMARY & CONCLUSIONS

A sub-critical, gas-cooled, fast reactor (GCFTR-2 [25]) with the primary objective of achieving > 90% burn of the TRU TRISO fuel was evaluated, and the secondary objective of achieving this without reprocessing the TRISO particles was investigated.

Operating sub-critically with a $k_{eff}^{BOC} = 0.95$ with a modest fusion neutron source strength of $P_{fusion}^{EOC} < 200$ MW limited the burn-up reactivity loss of the fuel such that repeated recycling with reprocessing proved to be the only possible fuel cycle scheme for this design.

By relaxing the constraints on k_{eff}^{BOC} and P_{fusion}^{EOC}, it was possible to evaluate other fuel cycles with respect to the primary and secondary objectives. A single-pass deep burn of 90% was performed which alleviated the necessity to recycle but required a P_{fusion}^{EOC} of approximately 3400 MW. Recycling without reprocessing (with a $k_{eff}^{BOC} = 0.86$) until > 90% burn was achieved was found to be possible, but inefficient – only 6% of the reactor feed mass composed of recycled fuel with the rest composed of fresh make-up feed.

In addition to the main objectives, availability was also a concern. It was desired to have cycle times of > 330 days. Under the k_{eff}^{BOC} and P_{fusion}^{EOC} constraints, recycling with reprocessing resulted in cycle times of 240 – 305 days, depending on the fuel path. Removing the k_{eff}^{BOC} constraint resulted in a 376 day cycle time. Recycling without reprocessing (also with the k_{eff}^{BOC} constraint removed) resulted in a 330 days fuel cycle. The single-pass 90% burn had a cycle time of 3000 days.

One hundred percent destruction of the TRUs was achieved at the rate of ~1.12 MT/FPY for all fuel cycles except for the single-pass fuel cycle. This corresponds to the

disposal of ~100 MT SNF/FPY. A single reactor could "support" three 1000 MWe LWRs and a fleet of 35 reactors could support the entire U.S. nuclear reactor fleet at current levels of power production.

The recommended design changes are (1) larger fusion power source and (2) larger core volume. The larger fusion power source will allow for a lower k_{eff}^{BOC} which will in turn allow for a higher fraction of low-reactivity recycled fuel in the reactor feed stream and a larger burn-up per pass. Larger core volume will allow for a larger fraction of the reactor feed stream to be composed of low-reactivity recycled fuel. Both changes would also allow for longer cycle times (thus greater availability).

A more accurate recycle-without-reprocessing scenario should be performed in which the TRISOs are removed from the burn cycle at 90% burn rather than remaining in the burn cycle. This will increase the recycled fuel volume fraction in the reactor feed.

The isotopic distribution of the TRU fuel was calculated at several time steps up to 90% burn-up to evaluate the assumption used for recycling-with-reprocessing. It was found that the overall trend is toward less reactivity than that implicit in the assumption of constant TRU isotopic composition during irradiation. Further research needs to be done to determine the impact of the changing isotopic composition of reprocessed fuel. A reprocessing fuel cycle that accounts for the isotopic change should be performed.

The conventional TRISO fast fluence limit of 4-8E+21 n/cm^2 is exceeded by all the fuel cycles in this study. However, this design used a modified TRISO to anticipate a large fast fluence. Further research into the radiation and pressure limits of the modified TRISO should be performed.

APPENDIX A: Computation Model
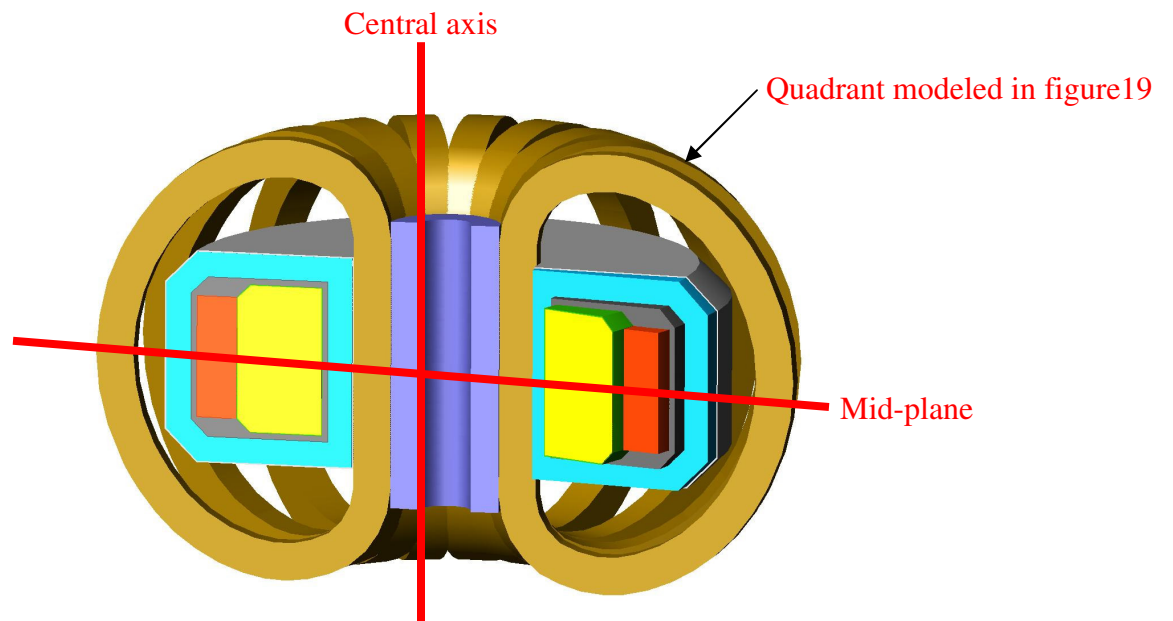
Figure 18. Reactor symmetry.

Outer R	66	136	179	185	246	261	264.5	480.5	484	508.4	531.6	553.9	575.3	596	611	672	678	721
Upper Z																		

Regions (upper half, R-Z geometry):

- Upper Magnet (Z 312)
- Upper Vacuum Vessel (Z 269)
- Upper Shield (Z 263)
- Upper Reflector (Z 202)
- Central Reflector
- Void
- Central Solenoid
- Inner Magnet
- Inner Vacuum Vessel
- Inner Shield
- Inner Reflector
- Inner First Wall
- Upper First Wall
- Plasma
- Outer First Wall
- Outer Refl
- Outer Shield
- Outer Vacuum Vessel
- Outer Magnet

Z					
150	Core5e	Core4e	Core3e	Core2e	Core1e
120	Core5d	Core4d	Core3d	Core2d	Core1d
90	Core5c	Core4c	Core3c	Core2c	Core1c
60	Core5b	Core4b	Core3b	Core2b	Core1b
30	Core5a	Core4a	Core3a	Core2a	Core1a

Figure 19. Computational model.

This is a model of the upper half of the reactor in R-Z geometry. (not to scale)
All measurements are in centimeters.

The reactor was modeled in REBUS-3 with R-Z geometry. Only the upper right quarter (above the mid-plane and to the right of the central axis) was modeled (figure 18), taking advantage of the symmetry of the design.

The various regions shown were identified by specifying their radial and axial extents relative to the axis and mid-plane, respectively. For example, the upper first wall extends from 264.5 cm to 480.5 cm to the right of the axis and from 183.5 cm to 187 cm from the mid-plane. All regions were approximated by rectangles including the highly-curved magnets which were modeled as rectilinear regions wrapping around the outside of the vacuum vessel. Regions that elbowed had to be broken up.

The R-Z model consists of the rotation about the central axis of a 2-D cross-section of the upper half of the reactor with the following boundary conditions: Reflecting boundary conditions were used at the reactor mid-plane and central axis, and vacuum boundary conditions were used at the edges of the reactor.

The materials listed in table 2 of the text were assigned to the regions defined in figure 19.

APPENDIX B: Lithium (n, α) Cross Sections

Energy group	Lower bound (eV)	Upper bound (eV)	(n,a) cross section Li6	(n,a) cross section Li7
1	1.40000E+07	1.41910E+07	0.032540221	0.263177105
2	1.00000E+07	1.40000E+07	0.037137528	0.353134832
3	6.06530E+06	1.00000E+07	0.056321298	0.371769427
4	3.67880E+06	6.06530E+06	0.095230858	0.08183712
5	2.23130E+06	3.67880E+06	0.190540643	2.52036E-08
6	1.35340E+06	2.23130E+06	0.212035767	0
7	8.20850E+05	1.35340E+06	0.228235676	0
8	4.97870E+05	8.20850E+05	0.294990388	0
9	3.01970E+05	4.97870E+05	0.644319295	0
10	1.83160E+05	3.01970E+05	2.270697309	0
11	1.11090E+05	1.83160E+05	0.889202934	0
12	6.73790E+04	1.11090E+05	0.653108449	0
13	4.08680E+04	6.73790E+04	0.705500152	0
14	2.47880E+04	4.08680E+04	0.868859316	0
15	1.50340E+04	2.47880E+04	1.072156552	0
16	9.11880E+03	1.50340E+04	1.374482504	0
17	5.53080E+03	9.11880E+03	1.838303957	0
18	3.35460E+03	5.53080E+03	2.239817068	0
19	2.03470E+03	3.35460E+03	2.936858942	0
20	1.23410E+03	2.03470E+03	3.711365237	0
21	7.48520E+02	1.23410E+03	4.679825756	0
22	4.54000E+02	7.48520E+02	6.095516101	0
23	2.75360E+02	4.54000E+02	7.692306554	0
24	1.67020E+02	2.75360E+02	9.766822764	0
25	1.01300E+02	1.67020E+02	12.50150279	0
26	6.14420E+01	1.01300E+02	15.92304274	0
27	3.72670E+01	6.14420E+01	20.86430808	0
28	2.26030E+01	3.72670E+01	27.99197823	0
29	13.71	22.603	34.39696003	0
30	8.3153	13.71	45.81247501	0
31	3.9279	8.3153	61.96518667	0
32	0.53158	3.9279	99.39381818	0
33	0.414	0.53158	239.5773339	0
34	0	0.414	833.4	0

APPENDIX C: LWR SNF Composition [14]

Isotope	Moles/MTU SNF	Isotope	Moles/MTU SNF	Isotope	Moles/MTU SNF
th230	5.82E-05	se76	4.75E-05	ru99	3.08E-04
th232	1.31E-05	se77	1.01E-02	mo100	9.37E+00
pa231	2.21E-06	se78	3.30E-02	ru100	1.04E+00
u232	3.42E-06	se79	6.16E-02	ru101	7.63E+00
u233	2.53E-05	br79	1.86E-07	ru102	7.68E+00
u234	8.18E-01	se80	1.68E-01	rh102	1.27E-05
u235	3.63E+01	kr80	7.22E-07	rh103	4.06E+00
u236	1.66E+01	br81	2.45E-01	ru104	5.33E+00
u238	3.96E+03	kr81	5.31E-08	pd104	2.01E+00
np237	2.03E+00	se82	3.93E-01	pd105	3.71E+00
pu238	5.80E-01	kr82	7.78E-03	ru106	1.68E+00
pu239	2.51E+01	kr83	4.98E-01	pd106	1.90E+00
pu240	9.86E+00	kr84	1.35E+00	pd107	2.14E+00
pu241	1.79E+00	kr85	2.65E-01	ag107	2.22E-07
pu242	2.15E+00	rb85	1.07E+00	pd108	1.38E+00
pu244	7.29E-05	kr86	2.12E+00	ag108m	2.04E-06
am241	4.24E+00	sr86	4.05E-03	cd108	2.08E-06
am242m	3.07E-03	rb87	2.74E+00	ag109	8.38E-01
am243	4.69E-01	sr87	2.05E-05	pd110	4.05E-01
cm242	8.05E-06	sr88	3.86E+00	cd110	3.60E-01
cm243	8.13E-04	y89	4.76E+00	cd111	2.05E-01
cm244	5.28E-02	sr90	5.96E+00	cd112	1.06E-01
cm245	5.69E-03	y90	1.62E-03	cd113	9.50E-04
cm246	4.50E-04	zr90	2.19E-01	cd113m	1.17E-03
cm247	4.54E-06	zr91	5.97E+00	in113	5.57E-05
h3	1.68E-02	zr92	6.87E+00	cd114	1.08E-01
li6	3.30E-05	zr93	5.02E+00	sn114	2.85E-06
li7	1.46E-06	nb93	2.35E-07	in115	1.34E-02
be9	2.18E-06	nb90m	3.05E-06	sn115	1.55E-03
be10	1.31E-05	zr94	8.10E+00	cd116	4.35E-02
c14	1.89E-06	nb94	5.11E-06	sn116	1.90E-02
zn70	1.21E-07	mo95	6.70E+00	sn117	4.07E-02
ga71	1.15E-06	zr96	8.36E+00	sn118	3.25E-02
ge72	6.94E-05	mo96	3.74E-01	sn119	3.36E-02
ge73	2.02E-04	mo97	7.83E+00	sn120	2.38E-02
ge74	1.72E-04	mo98	8.43E+00	sn121m	3.63E-04
as75	1.51E-03	tc98	7.28E-05	sb121	3.24E-02
ge76	4.53E-03	tc99	7.89E+00	sn122	4.17E-02

Isotope	Moles/MTU SNF	Isotope	Moles/MTU SNF
te122	2.16E-03	pm145	1.70E-07
sb123	3.69E-02	nd146	4.73E+00
te123	1.83E-05	pm146	6.06E-05
sn124	6.86E-02	sm146	3.99E-05
te124	1.57E-03	pm147	1.21E+00
sb125	6.32E-02	sm147	4.37E-01
te125	1.94E-02	nd148	2.48E+00
te125m	7.70E-04	sm148	7.70E-01
sn126	1.55E-01	sm149	1.87E-02
te126	2.85E-03	nd150	1.20E+00
i127	3.24E-01	sm150	2.08E+00
te128	7.10E-01	sm151	1.13E-01
xe128	2.01E-02	eu151	1.09E-04
i129	1.40E+00	sm152	8.57E-01
xe129	1.13E-04	eu152	2.52E-04
te130	2.80E+00	gd152	3.36E-04
xe130	5.39E-02	eu153	7.79E-01
xe131	3.14E+00	sm154	2.44E-01
xe132	8.31E+00	eu154	1.63E-01
ba132	1.82E-06	gd154	1.07E-02
cs133	8.51E+00	eu155	3.63E-02
xe134	1.13E+01	gd155	2.74E-04
cs134	8.91E-01	gd156	4.52E-01
ba134	2.71E-01	gd157	7.76E-04
cs135	2.52E+00	gd158	1.18E-01
ba135	2.07E-03	tb159	1.50E-02
xe136	1.70E+01	gd160	6.54E-03
ba136	1.20E-01	dy160	1.13E-03
cs137	9.10E+00	dy161	2.20E-03
ba137	2.80E-01	dy162	1.68E-03
ba137m	1.40E-06	dy163	1.34E-03
ba138	9.30E+00	dy164	3.06E-04
la138	6.19E-05	ho165	3.96E-04
la139	8.70E+00	ho166m	1.37E-06
ce140	8.93E+00	er166	8.74E-05
pr141	7.49E+00	er167	1.71E-06
ce142	7.94E+00	er168	2.09E-06
nd142	1.30E-01	tm169	1.89E-08
nd143	5.57E+00	er170	2.09E-08
ce144	2.64E+00	yb171	7.73E-09
nd144	6.25E+00	yb172	1.76E-08
nd145	4.61E+00		

APPENDIX D: Fast Spectrum Analysis

Stacey et al. [23, 24] used a fast spectrum rather than a thermal one because although TRUs generally have larger fission cross-sections in a thermal neutron spectrum, they also have a larger capture to fission ratio, α, which will tend to produce more TRUs rather than destroy them. Conversely, a fast spectrum will result in lower fission cross-sections and lower α ratios which are more suited to the destruction of TRUs. Figure 21 displays this trend for the principle TRU isotope, Pu239. This trend is more acute for many of the other principal SNF isotopes (Pu240, Pu242, Np237, Am241) where thermal capture cross-sections actually exceed thermal fission cross-sections (see figure 22).
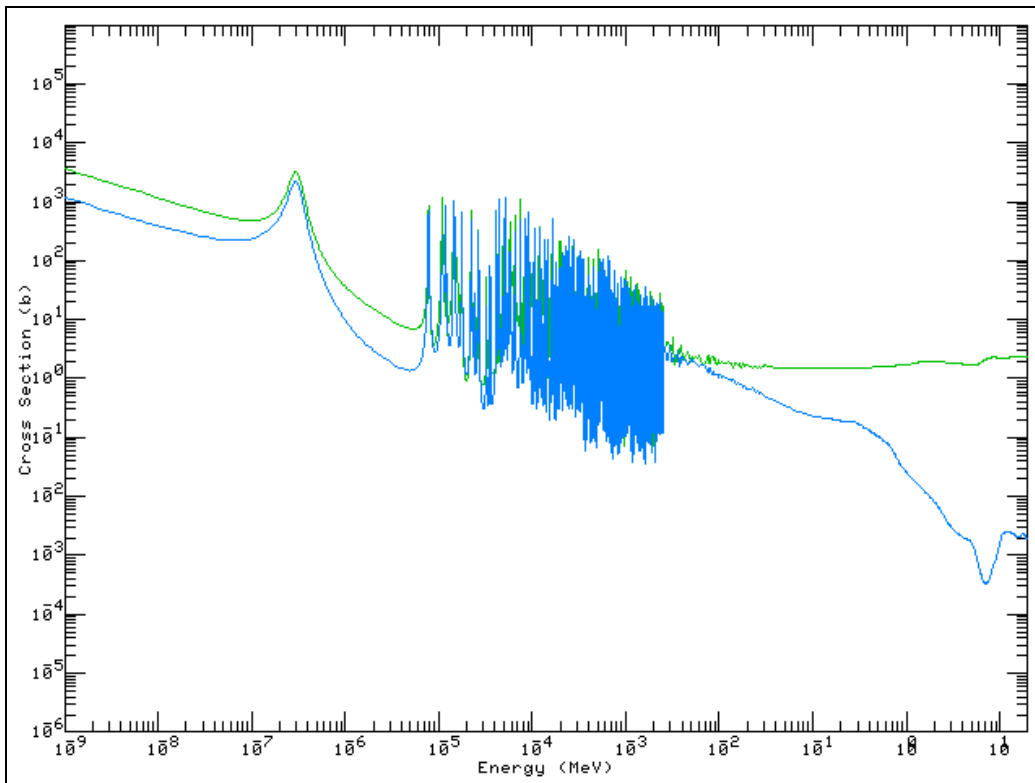
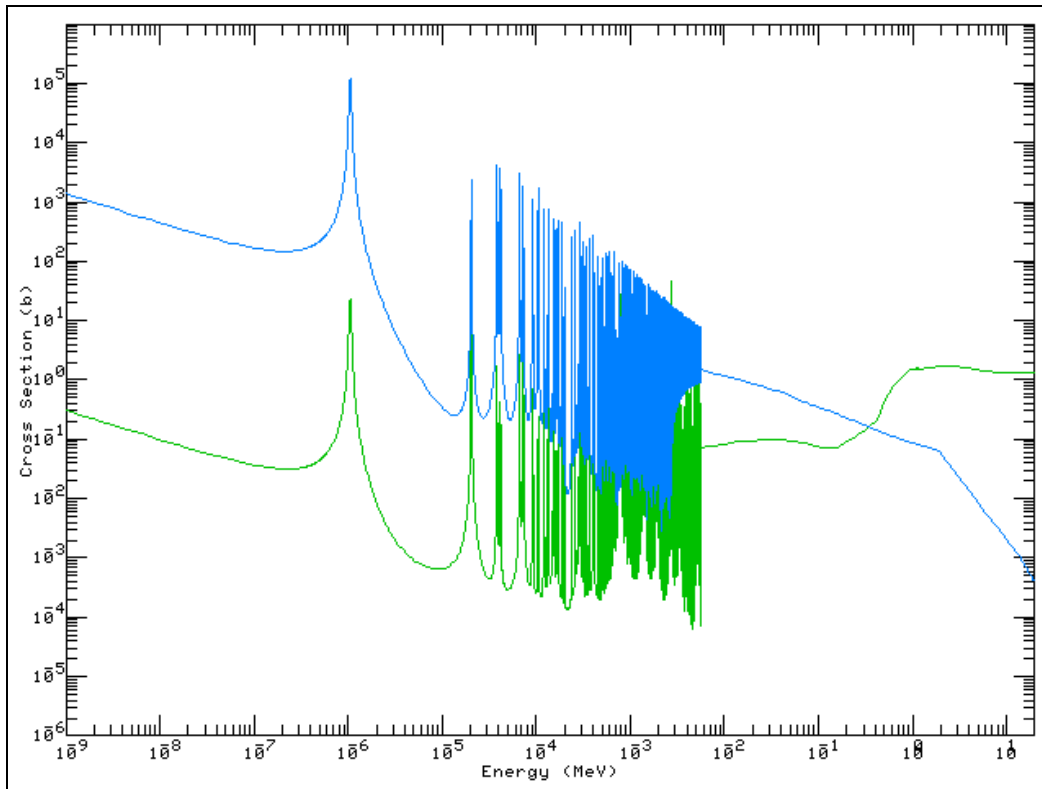**Figure 21. Pu239 Cross-sections (green=fission, blue=capture). [31]**

Figure 22. Pu240 Cross-sections (green=fission, blue=capture). [31]

REFERENCES

1.   "A Roadmap for Developing Accelerator Transmutation of Waste (ATW) Technology," DOE/RW0-519, U.S. Department of Energy (1999).

2.   E. A. Hoffman and W. M. Stacey, "Comparative Fuel Cycle Analysis of Critical and Subcritical Fast Reactor Transmutation Systems," Nuclear Technology, 144, 83 (2003).

3.   Stacey, W. M. Nuclear Reactor Physics. New York: John Wiley & Sons, Inc, 2001.

4.   "First Phase P&T Systems Study: Status and Assessment Report on Actinide and Fission Product Partitioning and Transmutation," OECD/NEA, Paris (1999).

5.   *Proc. 1ˢᵗ through 5ᵗʰ NEA International Exchange Meetings,* OECD/NEA, Paris (1990, 1992, 1994, 1996, 1998).

6.   "Nuclear Wastes–Technologies for Separations and Transmutations," National Research Council, National Academy Press, Washington (1996).

7.   C. D. Bowman et al., "Nuclear Energy Generation and Waste Transmutation Using Accelerator-Driven Intense Thermal Neutron Source," *Nucl. Instrum. Methods A,* 320, 336 (1992).

8.   W. C. Sailor et al., "Comparison of Accelerator-Based with Reactor-Based Nuclear Waste Transmutation Schemes," *Prog. Nucl. Energy,* 28, 359 (1994).

9.   T. A. Parish and J. W. Davidson, "Reduction in the Toxicity of Fission Product Wastes Through Transmutation with Deuterium-Tritium Fusion Neutrons," *Nucl. Technol.,* 47, 324 (1980).

10. E. T. Cheng et al., "Actinide Transmutation with Small Tokamak Fusion Reactors," *Proc. Int. Conf. Evaluation of Emerging Nuclear Fuel Cycle Systems*, Versailles, France (1995).

11. Y.-K. M. Peng and E. T. Cheng, "Magnetic Fusion Driven Transmutation of Nuclear Wastes (FTW)," *J. Fusion Energy*, 12, 381 (1993).

12. E. T. Cheng and R. J. Cerbone, "Prospect of Nuclear Waste Transmutation and Power Production in Fusion Reactors," *Fusion Technol.*, 30, 1654 (1996).

13. Y. Gohar, "Fusion Option to Dispose of Spent Nuclear Fuel and Transuranic Elements," ANL/TD/TM00-09, Argonne National Laboratory (2000).

14. L. J. Qiu et al., "A Low Aspect Ratio Tokamak Transmutation System," *Nucl. Fusion*, 40, 629 (2000).

15. W. M. Stacey, "Capabilities of a DT Tokamak Fusion Neutron Source for Driving a Spent Nuclear Fuel Transmutation Reactor," *Nucl. Fusion*, 41, 135 (2001).

16. "Non-Electric Applications of Fusion," Final Report to FESAC, July 31, 2003.

17. Stacey, W. M. "Transmutation Missions for Fusion Neutron Sources," Fus. Eng. Des. to be published (submitted 2005).

18. Stacey, W. M., J. Mandrekas, E. A. Hoffman, "Sub-critical Transmutation Reactors with Tokamak Fusion Neutron Sources," Fusion Science and Technology, 47, 1210 (2005).

19. Stacey, W. M., J. Mandrekas, et al. "A Fusion Transmutation of Waste Reactor," Fusion Science and Technology, Vol. 41, pp. 116-139 (March 2002).

20. Jassby, D. L. and J. A. Schmidt, "Electrical Energy Requirements for ATW and Fusion Neutrons," Fusion Science and Technology, 40 52-55 (July 2001).

21. LaBar, M. P. "The Gas Turbine – Modular helium Reator: A Promising Option for Near Term Deployment," GA-A23952 (April 2002).

22. Rodriguez, C., A. Baxter, D. McEachern, M. Fikani and F. Venneri. "Deep-Burn: Making Nuclear Waste Transmutation Practical," Nuclear Engineering and Design 2805 (2003) 1-19.

23. D. A. Petti, J. Buongiorno, J. T. Maki, R. R. Hobbins, G. K. Miller, "Key Differences in the Fabrication, Irradiation and High Temperature Accident Testing of U.S. and German TRISO-coated Particle Fuel, and their Implications on Fuel Performance," Nucl. Eng. Des., 222, 281-297 (2003).

24. W. M. Stacey, et al., "A Sub-critical, Gas-cooled, Fast Transmutation Reactor (GCFTR) with a Fusion Neutron Source," Nuclear Technology, 150, 162 (May 2005).

25. W. M. Stacey, et al., "A Deep-Burn, Sub-critical, Gas-cooled Fast Transmutation Reactor," Nuclear Technology, submitted (2005).

26. M. Kubota, Y. Morita, I. Yamaguchi, I. Yamagishi, T. Fujiwara, M. Watanabe, "Development of the Four Group Partitioning Process at JAERI," Fifth OECD/NEA Information Exchange Meeting on Actinide and Fission Product Partitioning and Transmutation, Session 2, pp. 1-9 (1998).

27.   B. J. Toppel, "A User's Guide to the REBUS-3 Fuel Cycle Analysis Capability," ANL- 83-2, Argonne National Lab (1983).

28.   "DANTSYS: A Diffusion Accelerated Neutral Particle Transport Code System," LA-   12969-M Manual UC-705, Los Alamos National Lab (1997).

29.   H. Henryson, et al., "MC2-2: A Code to Calculate Fast Neutron Spectra and Multigroup Cross Sections," Argonne National Lab report ANL-8144 (1976).

30.   Personal communication. Donald McEachern, General Atomics, 2005.

31.   http://atom.kaeri.re.kr/ton/nuc8.html (August 2005).